Wearable Sensor System for Quantifying Proprioceptive Competence in Microgravity

by

Shu-Yu (Michelle) Lin

B.S. in Aerospace Engineering Sciences
B.S. in Applied Mathematics
University of Colorado Boulder (2021)

Submitted to the Department of Aeronautics and Astronautics
in partial fulfillment of the requirements for the degree of

Master of Science in Aeronautics and Astronautics

at the

MASSACHUSETTS INSTITUTE OF TECHNOLOGY

June 2023

Authored by: Shu-Yu (Michelle) Lin
           Department of Aeronautics and Astronautics
           May 23, 2023

Certified by: Katya Arquilla
           Boeing Assistant Professor of Aeronautics and Astronautics
           Thesis Supervisor

Accepted by: Jonathan P. How
           R. C. Maclaurin Professor of Aeronautics and Astronautics
           Chair, Graduate Program Committee

Wearable Sensor System for Quantifying Proprioceptive Competence in Microgravity

by

Shu-Yu (Michelle) Lin

Submitted to the Department of Aeronautics and Astronautics
on May 23, 2023, in Partial Fulfillment of the
Requirements for the degree of
Master of Science in Aeronautics and Astronautics

Abstract

Microgravity poses a significant challenge for our neurovestibular and proprioceptive systems. Past spaceflight and parabolic research have shown degraded movement control upon microgravity exposure and adaptation of performance with time. However, most research does not address the functional, dynamic, whole-body movements we expect in spaceflight. In particular, as commercial microgravity experiences become ubiquitous, maladapted proprioceptive systems in novice flyers pose risks to themselves, other crew members, and expensive spacecraft equipment. We propose a framework to assess proprioceptive competence (introduced and defined in this thesis) through the metric of *fluidity*, a biomechanical property often used in medical rehabilitation and functional gait assessment. We designed, built, and pilot tested a wearable sensor system capable of inertial motion capture in the parabolic flight environment. Through comparing whole-body joint fluidity in translation movements done in 1-g and microgravity, we found evidence suggesting an increased fluidity upon entry into microgravity and increased fluidity throughout microgravity exposure.

Thesis Supervisor: Katya Arquilla
Assistant Professor
Aeronautics and Astronautics

Acknowledgments

I would like to thank my thesis supervisor, Katya. Throughout the last two years, I have gained so much from Katya's consistent mentorship and guidance. She inspires me to be rigorous, thoughtful, and intentional in my research, while at the same time curating my life with what brings me joy and fulfillment. I hope to continue learning from her and I am incredibly grateful for the relationship we have built together.

The parabolic flight was a milestone in my aerospace career and I am looking forward to many more. Thank you to Ariel Ekblaw, Jeffrey Hoffman, Sean Auffinger, Al Antonsca, and the Zero Gravity Corporation team for making the experience possible. I would like to thank my two undergraduate research assistants, Anna Yang and Caitlin Lian, for working with me on the development of the garment system and data analysis, respectively. As a first-time mentor, I could not have found more motivated and understanding students. I would like to thank my communities at the Space Exploration Initiative, SpaceX, Blue Origin, and NASA for giving their time generously to our thought-provoking conversations. To my labmates at the HSL, thank you for your camaraderie and friendship.

Thank you to my dear friends near and far. Thank you to Haruka and Sulli, my first roommates in Cambridge, for our wonderful connection that spans continents. This past year, I had the tremendous privilege of working at East Campus as a GRA. I would like to thank the house team, my students on 1E, and EC for being in authentic community together. Thank you to Kate, Makena, Annette, Elizabeth, and Lisa for filling my life so beautifully with your presences. Thank you to Björn for your empathy, commitment, and shared laughter. I feel immensely lucky that we get to walk our paths together. Special thank you to my sweet cat, Lilith, for her constant companionship. Fate brought us together and I am looking forward to a lifetime together.

Finally, thank you to my family. I am especially inspired by my siblings and their thoughtfulness, humor, and joy. It has been one of my greatest joys to watch them grow up and I look forward to experiencing all phases of life together. Thank you to my family in Taiwan for always welcoming me home with open arms. Despite oceans in between us, you are close in my heart.

感謝默默支持與關心我的家人，謝謝你們對我的信念與包容．在這個里程碑跟你們分享這份喜悅，還有三年的路要走，希望你們也可以一直陪伴著我．有你們我好幸福！

林書宇 謹致

Contents

List of Figures

List of Tables

Chapter 1

Introduction

In this chapter, we motivate the research by introducing relevant research gaps and the opportunity to understand whole-body proprioceptive changes due to microgravity. We discuss the existing technological platform of parabolic flights, wearable technology, and low-frequency sensor data to which our work is complementary. Finally, we introduce the fluidity framework as a novel approach to evaluate proprioceptive adaptation in microgravity, along with further potential applications of this framework.

1.1 Motivation and Background

1.1.1 Scientific Gap

Microgravity poses a significant challenge for human physiology. Research and operational evidence have demonstrated an alteration in vestibular and sensorimotor performance in microgravity, which have manifested as changes in visual acuity, hand-eye coordination, spatial orientation perception, postural control, locomotor ability, cognitive function, and perception [5][26]. Control of space systems (e.g. vehicles, rovers, control panels) is a high-level integrative function of the central nervous system (CNS), which relies on neural pathways that have developed and evolved under

Earth gravity [24][26]. The proprioceptive system, a complex system that is responsible for the control and awareness of our movements, is a CNS subsystem affected in microgravity which leads to decrements in coordination, perception, and postural/locomotion control [24][34]. Functionally, these performance decrements create risks in impaired control of spacecraft, vehicles, and other systems during spaceflight.

The full extent of the risk of adverse consequences due to vestibular and sensorimotor alterations associated with spaceflight is not fully characterized. Flight-analogs (e.g. parabolic flight) and ground-based research (e.g. tilt-translation) have mostly focused on the physiological sub-issues of oculomotor control, hand-eye coordination, and spatial orientation [26]. Partly due to their strong legacy in ground-based neuroscience and biomechanics research, experiments on the Vestibulo-Ocular Reflex, pointing movements, reaching, grasping, force discrimination and control, center-of-gravity control, and manual tracking are well-represented in the spaceflight research done to date [9][21][26][27][28][29][32][33]. While these findings provide insight into the neurological pathways and altered kinematics that underlie observed decreased performance and corroborate the crew verbal reports, they have limited extrapolatory power to functional and operational impacts during spaceflight [26]. From existing evidence obtained through pre/during/post-flight scientific investigations and from space flight operations, NASA has determined a basis for concern regarding vestibular/sensorimotor (including proprioceptive) adaptation to spaceflight, as well as justification for continued research in these areas [5][26][32][35].

Specifically, full-body locomotion and related functional implications in microgravity and gravity transitions remain knowledge gaps for both short-duration commercial space tourism and long-duration exploration mission design. When first encountering an altered gravity environment, arm movements are often inappropriate and inaccurate, suggesting similar maladaptation for full-body movements as well [14][17][23]. Past spaceflight research has shown that motor control strategies adapt after approx-

imately four weeks in the microgravity environment [22]. Furthermore, in the new age of space commercialization, spaceflight participants receive as little as 14 hours of training over two days before an 11-minute flight with three minutes of microgravity at the apex [25]. For many of the passengers, this is their first time experiencing microgravity, since a parabolic flight experience is not a part of the required training protocol. Therefore, initial proprioceptive response on a whole-body level is important to characterize for two reasons:

1. Contribute to the body of knowledge of physiological adaptations to microgravity

2. Inform design of spaceflight participant peripherals (spacesuits, capsules, seats, displays, controls)

The shortened flight time condenses high risk critical events (such as launch and landing), where the passengers may not be ready to perform the needed movements during contingency scenarios. For example, the NASA Crew Escape Systems manual highlights several emergency egress modes out of the crew capsule, where tasks such as egressing seats and hatches may be applicable to commercial spaceflight systems [10]. Nominal tasks in suborbital tourism flights may include egressing and ingressing seats, microgravity acrobatics (e.g. somersaults), and translating within the cabin. In a confined volume with sensitive instrumentation and screens, degraded proprioception creates higher risk to crew and vehicle health [39]. Dynamic whole-body movements are of particular interest and the focus of this thesis, since they are gravity-dependent and a primary function during microgravity [8]. A parabolic flight of 20 parabolas, each at 20 seconds, serves as an appropriate analog to a two-to-three-minute suborbital flight. **We aim to characterize the response and subsequent adaptation of the proprioceptive system during short-duration microgravity exposure through a parabolic flight campaign.**

1.1.2 Technological Gap

Studying proprioceptive adaptation requires technology that allows the capture of detailed and accurate motion data across the body. Motion tracking is used in a wide range of terrestrial applications, from medical research, to athlete performance evaluations, to CGI (computer-generated imagery) for the entertainment industry. Motion tracking can be done optically or non-optically (inertial, magnetic, and mechanical) [20]. For the context of this project, we will only choose to explore inertial motion capture out of all non-optical solutions since it is the most common. Inertial motion capture utilizes motion sensors, usually in the form of Inertial Measurement Units (IMUs), which contain a three-axis accelerometer, three-axis gyroscope, and three-axis magnetometer. IMUs can capture full six degrees-of-freedom motion with respect to an inertial reference frame provided by the magnetometer which measures with respect to the Earth's magnetic field. Optical motion capture utilizes software (usually developed in-house by the companies) that can recognize visual markers (such as colored dots) and differentiate their spatial positions with respect to each other. Table 1.1 provides a summary of the advantages and disadvantages of each strategy.

Table 1.1: Comparison of inertial vs. optical motion capture systems.

Motion Capture Systems		
Solution	Advantages	Disadvantages
Inertial	Cheaper	Difficult to visualize
	Does not need line of sight	Requires inertial frame
	Raw data	Noisy
Optical	Extreme accuracy (< 0.2 mm [3])	Expensive
	Portable	Software interface
		Requires clear line of sight

Collecting data in the spaceflight environment is difficult and constrained by operational feasibility (mass, volume, power, minimal hazards, crew time, crew workload, competing schedules). Although the constraints on a parabolic flight are different,

10

optical tracking is still operationally difficult. Payloads and projects are placed close to each other during the experiment. Novice participants have difficulties staying in the confined volume dedicated to their projects. Optical systems require a clear line of sight for continuous tracking and the chaotic flight environment would likely interrupt data collection.

To overcome these challenges, we propose a wearable sensor system that performs inertial motion tracking. Wearable sensor systems have been leveraged in biomedical research, such as for gait assessment. Asakura et al. quantified fluidity in a sit-to-walk test at 100 Hz to demonstrate clinical utility of accelerometer data in elderly individuals or patient populations [2]. Lee and Tang demonstrated a wearable motion tracking system using 10 IMUs at 59 Hz for gait analysis during rehabilitation [19]. Wearable systems have also been used in the space domain. Fineman et al. measured biomechanical performance to assess spacesuit fit at 128 Hz using five IMUs mounted on the legs and five mounted on the spacesuit [12]. Finally, a wrist-mounted wearable sensor collecting three-axis accelerometer data at 32 Hz was used by Johnson et al. on a parabolic flight to characterize movement [16]. All of these wearable sensor systems demonstrate the feasibility of inertial motion capture in our targeted operational environment for a whole-body movement task at relatively low frequencies ($\approx$ or $<$ 100 Hz).

1.2 Fluidity Framework

Proprioceptive adaptions in microgravity are more holistically understood in the context of a broader set of physical adaptations. In Figure 1-1, physical instinct is shown as the largest circle, representing all physical and physiological adaptations from the headward fluid shift to muscle atrophy [24]. We are interested in the proprioceptive system, in particular its functional performance in microgravity. **Here, we intro-**

duce and define proprioceptive competence:

1. **Adaptability to novel environments**

2. **Capability of sustaining nominal tasks in the given environment**

Definition 1.2.1 (Proprioceptive Competence). Proprioceptive competence is one's adaptability to novel environments and capability of sustaining nominal tasks in the given environment, as related to movement.

As an example, there is evidence of proprioceptive competence in the adaptation and sustained employment of fine-control strategies during a set of 50 traverses during parabolic flight [39]. Finally, fluidity is proposed as the metric by which to measure proprioceptive competence. Camurri et al. proposed a multi-layer framework that describes the tiers of movement quality in increasing order of complexity; layer 1 involves kinematics (joint trajectories), layer 2 is the biomechanical feature of joints at a small time scale (smoothness), and layer 3 is the complex quality prescribed to a longer duration of movement (rhythm, flow) [7]. Previous work by Piana et al. utilized this multilayer framework to create a measurable definition of fluidity, which was based on the minimum-jerk theory proposed by Flash and Hogan [13][31]. We propose a modification to the fluidity definition provided by Piana et al. The full derivation can be found in Chapter 3.3.2.

$$\text{FI} = \frac{n}{\Sigma(|j_i| + 1)}, \ 0 \leq i \leq n \tag{1.1}$$

The Fluidity Index (FI) of the trajectory of a joint is defined in Equation 1.1 where j_i is the jerk at time index i, $0 \leq i \leq n$.
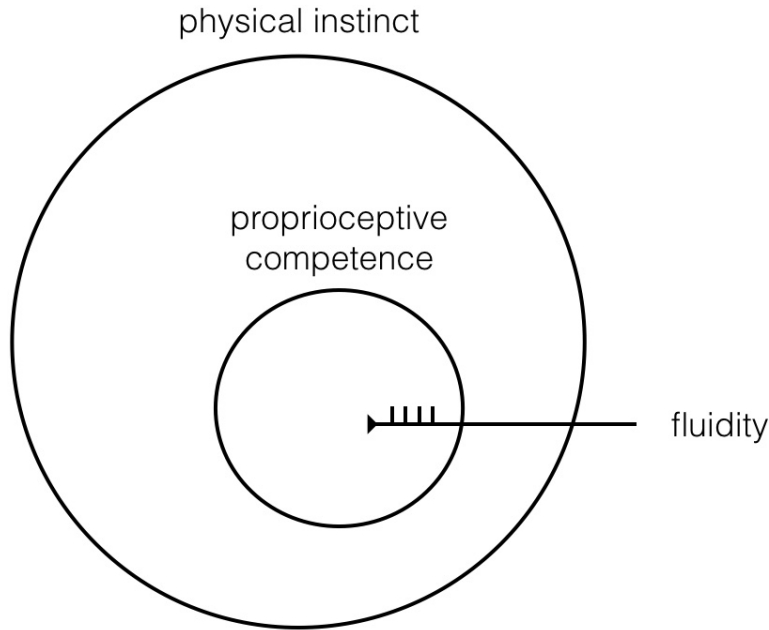
Figure 1-1: Proprioceptive competence, which we are defining here, is nested within all physical instinct (e.g. fluid shifts, cardiovascular changes, muscle atrophy in microgravity). Fluidity is proposed as a metric to measure proprioceptive competence, which has a two-part definition: adaptability to novel environments and capability of sustaining nominal tasks in the given environment.

1.2.1 Applications

We propose the following applications for the continuation of this research topic and framework:

Wearable technology for movement augmentation

Inadequate proprioceptive adaptation poses risks for equipment damage and crewmember injuries for short-duration flights [39]. In more complex mission architectures to the Moon and Mars with repeated transitions from partial gravity to microgravity environments, this risk is exacerbated [5]. This framework drove the development of a wearable sensor system to quantify fluidity, and this system can be leveraged in the future for crewmember training and to inform wearable technology for augmenting

movements to prevent injuries.

Future space habitat and suit design

Our framework introduces an approach to quantifying the microgravity experience through continuous monitoring of the participant's interactions with the environment; furthering this approach, the same type of continuous measurement could be used to evaluate different space habitats in virtual and augmented reality environments. Space habitat design has traditionally been challenged by the time and material costs of developing full mock-ups to assess alternative designs. Virtual and augmented reality have been used to mitigate these issues, but they rely on discrete measurements of user experience [4]. This proposed approach could be integrated into future high-frequency commercial spaceflight missions to augment our understanding of the human response to microgravity to refine spacecraft interiors. Data about movement quality and proprioceptive adaptation are especially relevant to interior design for physical ergonomics and spacesuit design.

Integrating transdisciplinary methods into bioastronautical engineering

Given the complexity of human experience and the many changes that occur upon entering microgravity environments, bioastronautical engineering has historically benefited from the influence of other research disciplines – textile designers have been key in the development of spacesuit soft goods, microbiologists lead research efforts to understand the spaceflight environment, psychologists investigate the impacts of the isolated, confined, extreme environment that is space, and more. Fluidity of motion is a concept that is qualitatively used in disciplines such as dance and the performing arts. Drawing inspiration from the humanities and arts can help engineers quantify, measure, and predict historically qualitative and abstract ideas to further the body of knowledge regarding human behavior.

1.3   Research Questions

Utilizing the fluidity framework, we can investigate proprioceptive competence in short-duration microgravity exposure. We pose the following research questions which guide the development of the garment technology, the experimental protocol, and the statistical analysis.

1. How does fluidity change upon introduction to microgravity?

2. How does fluidity change throughout short-duration microgravity exposure?

We will answer these research questions throughout this thesis.

Chapter 2

Development and Prototyping

In this chapter, we discuss the development and prototyping process of the garment system. We first describe the research constraints, namely the project timeline, the operational environment, and the scientific requirements following our experimental design. Then, we lay out system requirements and the two prototypes that were pursued after a commercial-off-the-shelf (COTS) technology evaluation. We also discuss electronic system integration to the garment, ergonomic considerations, and challenges encountered during the development process.

2.1 Research Requirements

2.1.1 Project Timeline

This project was selected to be developed within the project course "Prototyping our Sci-Fi Space Future: Designing & Deploying Projects for Zero Gravity Flights" cross-listed to MIT Media Lab (MAS.838) and MIT Aeronautics & Astronautics (16.88). The abbreviated course timeline is shown in Table 2.1. We were given a budget of $300 for project development.

The expected deliverable of the course was a fully built system that would be

demonstration-ready by Critical Design Review, which provided a three-month prototyping window. After the course ended in Fall 2021, students were expected to iterate on their projects so they were flight-ready by March, when the Payload Integration Package (PIP) was due. After the PIP was handed in to the flight provider, no further changes could be made.

Table 2.1: Abbreviated course timeline for project course "Prototyping our Sci-Fi Space Future: Designing & Deploying Projects for Zero Gravity Flights" (MAS.838/16.88)

Date	Deliverable
September 14, 2021	Research idea proposal
October 26, 2021	Preliminary Design Review: Motivation, system design, Concept of Operations, risk matrix and mitigation plan, schedule, budget subsystem demonstration
December 7, 2021	Critical Design Review: Full system design, Concept of Operations, experimental setup, full system demonstration
March 11, 2021	Payload Integration Package for flight provider: Hazards information, battery specifications, flight plan
May 20, 2022	Microgravity flight

2.1.2   Test Environment

The garment was designed for the parabolic plane environment, which posed challenging technical and operational constraints. Each microgravity parabola is around

20-30 seconds. In between them are hyper-gravity (1.8-2 g) portions where passengers must lie still. Our flight profile is shown in Table 2.2. Three minutes of experimentation time broken up into 20 second parabolas necessitates the flight operations to be streamlined and as simple as possible.

Table 2.2: Parabolic flight profile

Parabola number	Gravity level
1	Martian
2	Martian
3	Lunar
4	Lunar
5	Lunar
3 minute break	
6	Microgravity
7	Microgravity
8	Microgravity
9	Microgravity
10	Microgravity
10 minute break	
11	Microgravity
12	Microgravity
13	Microgravity
14	Microgravity
15	Microgravity
3 minute break	
16	Microgravity
17	Microgravity
18	Microgravity
19	Lunar
20	Lunar

Researchers departed Boston at 7am to Portsmouth, NH for the flight. Once all researchers and crew boarded the plane, the plane took off into a designated airspace and reached cruising altitude. From there, around 10 minutes of set-up time was allotted before the first set of parabolas. Referencing Table 2.2, there was a three-minute break every five parabolas, and a 10-minute break half-way through while the plane turned around to head toward the airport. The entire flight was around three hours. There was a two-hour debrief process before the bus back to Boston.

The flight environment is noisy and chaotic. Due to the number of projects flying in the same plane, space is constrained. While surrounded by other researchers, most of whom are novice flyers, it is likely that something unexpected (a limb, person, or part of an experiment) will enter one's designated or personal space. Therefore, wires and other free-floating accessories are strongly discouraged as they can present tangle hazards. Flyers can potentially bump into each other or bump against a surface, so any on-body systems should be able to sustain impacts without damaging the plane, the wearer, or other people. Due to the number of people in the cabin and the uncontrollable movements in microgravity, clear lines of sight are not guaranteed.

Parabolic flights can also be taxing on the body; gravity transitions, floating, and spinning sensations during microgravity can induce nausea and motion sickness [16]. Researchers are encouraged to simplify and automate the in-flight operations as much as possible while preserving research integrity to prevent getting sick.

Electrical and power limitations include no access to active power through outlets and no Bluetooth-enabled devices. Similar to a commercial plane, all devices must be in airplane mode. Any electrical or magnetic component must pass an EMF test on flight day.

Project requirements for the Zero Gravity Corporation (Virginia, US) parabolic flight were having a manual power switch, flight-certified batteries, and the ability to be worn underneath a Zero Gravity Corp. flight suit. Any systems that are secured or bolted to the plane floor must also demonstrate tolerance to 9 g's of load in all directions via structual analysis.

2.1.3 Scientific Requirements

Joint kinematics are well-established in biomechanical mathematical models [13][30][39]. COTS products also often utilize joint-tracking and mathematical models in both optical and inertial solutions. Furthermore, joints are more discrete options than limb

segments; 'elbow' is a clearer anthropometric marker than 'middle of the forearm'. Placing sensors at the joints allows for standardization across trials and studies. We chose accelerometers to be placed at all joints that are covered with a garment: shoulders, elbows, wrists, hips, knees, and ankles. Joints that are sometimes included in more comprehensive systems (head, neck, fingers) were not included due to the operational complexity of placing sensors outside of a garment system.

For our data collection, we opted for a data rate on the higher end based on the literature pursuing similar research goals. Data size was not a concern, since the amount of data we could collect was already constrained by the duration of the parabolic flight (13 parabolas with ≈ 20 seconds of microgravity each). A higher data rate can help maximize the signal-to-noise ratio, which is a concern in sensor-based studies and especially for cheaper COTS accelerometers. Johnson et al. collected three-axis accelerometer information at 32 Hz for parabolic flight, and Lee et al. performed gait analysis at 59 Hz with a self-developed motion tracking system [16][19]. For experiments on fluidity, Asakura et al. and Piana et al. both used 100 Hz [2][30]. For our baseline target frequency, we chose a 100 Hz data collection rate for each sensor in order to have sufficient flight data for fluidity analysis.

2.2 System Requirements

The design decisions for the garment system were motivated by the parabolic flight environment. The garment was designed to be self-sufficient, compact, wearable, and robust. For this particular project, self-sufficiency is such that the garment package will

- house an independent power supply

- collect data without user management (except to power on)

- not require any attachments or additional accessories to use (including laptop connections, extra batteries, external cameras, Bluetooth devices, straps, and other wearable systems)

To measure motion, we selected SparkFun's (Colorado, USA) 6 Degree-of-Freedom (DOF) Accelerometer, LSM6DSO. It measures three degrees of linear acceleration and three degrees of rotational motion. We chose a 6DOF accelerometer over an IMU since data from the magnetometer would not be captured in the flight environment, and IMUs were more expensive and scarcer than 6DOF accelerometers. The data from the sensors would be stored on a microSD card for post-flight analysis. Figure 2-1 is a representation of the proposed placement of accelerometers and other components. To minimize obstruction to motions for comfort, safety, and signal integrity, the placements of the systems were strategically chosen on the deltoids or top of the thighs.
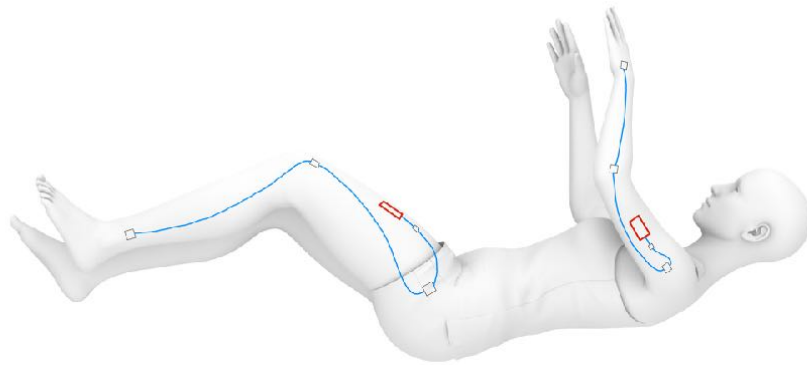

Figure 2-1: Representation of subsystem placement on a human model. Wires connect simplified subsystems (red boxes) and squares at each joint location represent the accelerometers.

2.3 COTS Motion Capture System Evaluation

We considered several COTS motion capture systems while determining which solution can best support the scientific goals. Table 2.3 shows a subset of popular inertial and optical systems we considered, along with their prices. Customer sales representatives quoted 6-12 cameras for a 3 by 3 by 3 meter space, tracking a single occupant with the goal of obtaining kinematic joint data. Inertial solutions would require at least 12 trackers, although most were sold in sets of 17 with the exception of Vicon's (Hauppauge, NY) Blue Trident. For our setup, all COTS solutions were at least several thousand US dollars, which was inaccessible for a pilot study of this scale in an educational research context. Beyond the visual occlusions from the chaotic flight environment preventing clear line of sight, we were also not permitted to mount cameras to the plane interior (only to other payloads). Therefore, optical systems were not considered viable solutions for our research.

Table 2.3: Commercially-available starter motion capture systems. [1]recommended by company representative [2]not commercially available at time of writing

Company	System	Type	Price
Movella	Awinda Starter	Inertial	$4590
	MVN Link full body suit[1]	Inertial	$14,920
Qualisys	Miqus	Optical	$6000 per camera
	MiqusM3[1] (8 cameras)	Optical	$58,000 total
Vicon	Blue Trident	Inertial	$1600 per tracker
OptiTrack	Flex 3 (8-12 cameras)	Optical	$660 per camera
	PrimeX 13[1] (8-12 cameras)	Optical	$2500 per camera
	PrimeX 22[1] (8-12 cameras)	Optical	$4000 per camera
Noitom	Perception Neuron Studio[1]	Inertial	$7500
	Perception Neuron 3	Inertial	$4000
	Perception Neuron Pro[2]	Inertial	$2000

We were able to obtain an educational loaner system of the Perception Neuron Pro from Noitom (Miami, FL). To utilize PN series systems, Noitom provides their data collection and visualization software for download. Through the system familiarization process, which took about an hour, we experienced key challenges. We

were unable to properly calibrate all 17 sensors simultaneously. During the flight, this would result in incomplete or missing data across one or more locations on the body. The calibration process also required a magnetic field, which was not feasible in the parabolic flight environment. PN Pro had an anti-mag mode, which would require re-calibration every five minutes in order to prevent excessive drift. With the flight profile, this would have compromised our data collection and research integrity. Additionally, the system required a computer and a relatively large empty area, which increased operational complexity.

We found that the feet were treated as contact points to the ground plane, which ensured postural and drift stability in a terrestrial setting. However, necessitating feet contact with the ground is not viable in our microgravity experimental setup. When we removed the feet-ground contact requirement in the settings, we noticed a steady positional drift of all sensors at a quick speed (roughly 1 meter/second). The training representative mentioned the addition of a "free climbing" mode in Perception Neuron Studio, which could resolve this issue. However, it would have only been available to loan for two weeks at a time, which impossibly constrained the prototyping and validation processes.

Some potential issues we explored in the training session that ultimately prevented us from using the system also included the possibility that the system may need to recalibrate and/or demagnetize. Given the condensed one-take nature of parabolic flights, these were risks we deemed too hazardous to mission success. Overall, we did not feel confident about the robustness of the sensors or the accuracy the system would be able to provide in the parabolic flight environment.

Due to the price point, operational limitations in the unique parabolic flight environment, and issues with utilizing the COTS equipment, we decided to prototype a custom wearable garment system.

2.4 Preliminary Prototype

The first prototype was designed and built in a three-month timeline due to the constraints of the project course. The course-provided materials served as a starting point for the hardware. This first system comprised of four RedBoards, the SparkFun microcontroller that interfaced with each component. Each RedBoard had three LSM6DSO 6-DOF accelerometers, an OpenLog, a 9V battery, and a multiplexer attached via the Qwiic system. Qwiic is a SparkFun-developed system that uses 4-pin JST connectors to "plug and play" with multiple compatible components and conducive to prototyping.
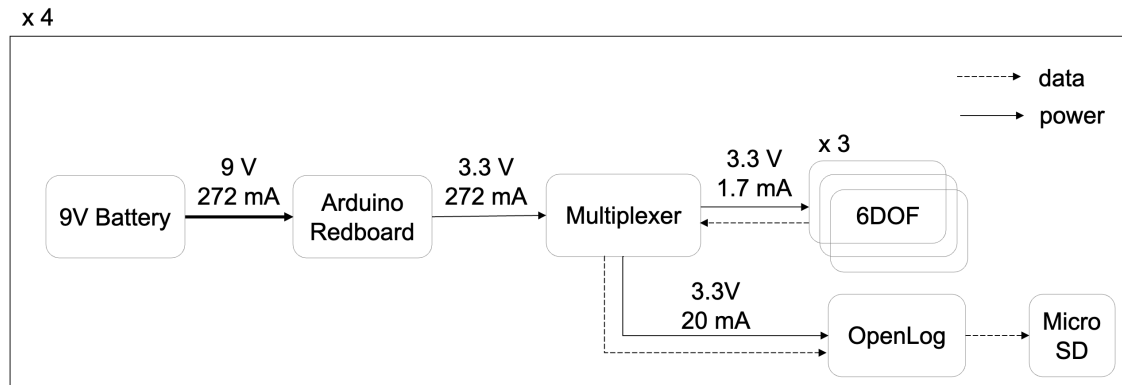
Figure 2-2: Simplified block diagram of the first prototype. Four of these subsystems comprised the full whole-body system. Power and data streams are shown with solid and dashed arrows, respectively.

Each subsystem (block diagram in Figure 2-2) corresponded to a limb, for a total of four subsystems with three accelerometers each. While each accelerometer address can be set to (0X6A) or (0X6B), there was an I2C address conflict with three identical components attached to the same I2C bus on the RedBoard. We chose to introduce a multiplexer instead of implementing an SPI protocol to preserve the advantages of the Qwiic system. The entire system was sewn by hand onto a black Capezio Ballet Makers Inc. (Totowa, NJ) unitard. Machine-sewing was not compatible since the tight elastic garment could not be stretched to fit a sewing machine. While

all measurements were made carefully to ensure symmetrical attachment, there will be variability in any attachment method (by hand or machine). The flexibility of the garment allows for on-body adjustments to ensure each sensor is in the optimal position for comfort and data collection. We accept the small differences present in the location of the sensors as inevitable consequences of a wearable system. The accelerometers' x-axes were aligned to be the body-x direction (pointing forward from the body). All accelerometers' z-axes were normal to the body surface.

Each subsystem was switched on by connecting the 9V battery with a battery clip and DC plug to the RedBoard. The RedBoard was loaded with a program and data collection started as power was provided. Therefore, all four independent subsystems did not start data collection at the same time and had asynchronous data timestamps.

Each sensor provided the following data string to the microcontroller: time (in milliseconds since powering on), the linear acceleration in x/y/z axes in 10,000*[g = fraction of 9.81 m/s^2], and the angular motion around the x/y/z axes in 10,000*[rad/s]. The 10,000 multiplier converts the data from the sensor with four decimal points from a floating point number to a signed integer which decreased processing speed.

string	13	685	2191	-9784	16275	-1400	-8050
	time	x-accel	y-accel	z-accel	x-gyro	y-gyro	z-gyro
units	ms		10,000*[g]			10,000*[rad/s]	

During full system validation, the prototype successfully turned on and collected data to the SD card at 13 Hz, a data rate that was constrained by the processing power of the RedBoard. While the targeted data speed of 100 Hz was not met, sensor communication and data collection were validated. Ergonomics was considered with all four systems attached. The protrusion of the system from the garment introduced risks of damaging the system and the user in the operational environment. The weight and placement of the systems on the limbs created hindrance to natural movement. The components were noticeably heavy and their large surface area contact with

the garment caused the fabric to sag and conformal fit was compromised. All four independent systems needed to be powered on separately and we noted that the manual operations took more effort and time than ideal. We aimed to decrease the number of independent systems and streamline the power-on process to ensure more accurate and simple flight operations. The 9V batteries were depleted after testing and demonstration, which revealed the need for a rechargeable battery with a larger capacity to support the second round of prototyping, testing, and flight.

2.5   Final Prototype

The main improvements we aimed to make and their corresponding tasks for the final prototype were:

- The battery should be rechargeable to prevent financial and energy waste.
  $\rightarrow$ New battery selection

- The overall footprint (the surface area that is in contact with the garment), weight, and profile (height protruding from the garment) of the system should be reduced to increase mobility and garment conformity.
  $\rightarrow$ New microcontroller

- Increase the data collection rate to 100 Hz from each sensor.
  $\rightarrow$ New microcontroller

- Decrease the number of independent subsystems from four to two.
  $\rightarrow$ New microcontroller

- Add a kill switch to be compliant with flight provider standards.
  $\rightarrow$ Add component

- Record absolute time for referencing sensor timestamps across independent systems.

  → Update software to include Real Time Clock (RTC)

2.5.1 Microcontroller Trade Study

To address the improvements for the final prototype, we conducted a trade study to determine a more suitable microcontroller choice, which has cascading implications to the rest of the component choices. The trade study considered the following criteria: cost, footprint, number of I2C buses, data processing speed, and microSD card compatibility. We considered the Teensy boards and the Raspberry Pi boards, both popular microelectronics boards for parabolic flight that were recommended to us by an avionics expert. Of all Teensy models, we selected the Teensy 4.1 for review since it had microSD card compatibility and the highest processing speed. The specifications of the microcontrollers under trade (with the RedBoard for reference) are summarized in Table 2.4 and the trade study scoring is displayed in Table 2.5.

Table 2.4: Specifications of the Raspberry Pi and Teensy 4.1 under trade study consideration. RedBoard is included for reference.

Specification	Raspberry Pi	Teensy 4.1	RedBoard
MicroSD slot	Yes	Yes	No
Power	3.3 V	3.3 V	3.3 V
Clock speed	**1-1.5 GHz**	600 MHz	16 MHz
I2C speed	400 kbit/sec	**1000 kbit/sec**	400 kbit/sec
# of I2C buses	2	**3**	1
Cost	**$25**	$29	$21
Footprint	36.4 cm^2	**10.8 cm^2**	36.5 cm^2

Table 2.5: Microcontroller trade study criteria, weights, and results.

Criteria	Weight	Raspberry Pi	Teensy 4.1
Clock speed	1.5	1	0.5
I2C speed	1.5	0.4	1
# of I2C buses	3	0.6	1
Cost	1	1	0.9
Footprint	3	0.6	0.9
Total	10	6.7	**8.9**

Following the trade study, **we selected the Teensy 4.1 as the microcontroller for the final prototype**.

2.5.2 Battery Sizing

The Teensy 4.1 usually consumes 100 mA [37]. In high performance mode, the 6DOF accelerometers consume around 0.55 mA each [38]. With six accelerometers per Teensy, this yields 103.3 mA. The microgravity flight is about three hours, and each system needs 309.9 mAh for a total of 619.8 mAh. We selected a 1000 mAh LiPo battery to provide a 1.5 factor of safety, a 85%-reduced profile from the 9V battery, and rechargeability. The LiPo battery was used to power both microcontrollers via a single power switch. The switch satisfied the flight provider requirement for a system kill switch and provided an advantage over prototype 1, which required four manual power switches when powering on the system.

2.5.3 System Build and Validation

The Teensy did not use Qwiic connections as the RedBoard did. Instead of interfacing with a single port, the 4-pin JST plug had to be spliced into wires in order to interface with individual pins on the Teensy board. The sensors still used Qwiic connections,

and the microcontroller end was spliced and soldered onto a solderable breadboard that held both microcontrollers and a manual power switch. The information flow remains consistent, but there was an added layer of complexity to splice and solder the connections onto the breadboard during the build process.

The Teensy microcontrollers were soldered onto the breadboard with break-apart headers. The wires from the Qwiic connectors all had plastic sheaths which were pulled apart and stripped, then passed through one hole on the breadboard before being soldered in another hole. This technique provided strain relief to the small solder joint. In a garment-integrated system, the fabric has more stretch than the electrical components. Therefore, while the fabric may easily accommodate motion due to its inherent elasticity, the same motions will cause strain in other components. Hot glue was placed on solder holes to prevent fatigue after verifying all connections with a multimeter.

To synchronize the two independent microcontrollers, the software was updated to include RTC capability on all timestamps. The RTC is set when the program is loaded into the microcontrollers, and supported by a coin cell battery so the time will remain accurate even when the system is not powered. The two systems shared one LiPo battery and one power switch, reducing the operation time by 75%.

Prior to soldering, we created a breadboard system and ran the program to ensure data collection. All of the components, including the LiPo battery, were represented and flight-like. After soldering, we laid out the garment and ran a three-hour static test to simulate the duration of the parabolic flight. We verified the test by checking for continuous data collection at 100 Hz from all sensors and ensuring all sensors were in absolute acceleration mode (one accelerometer axis stored ± 1 g) instead of relative acceleration mode (all accelerometer axes reading ≈ 0 g), since we were capturing data across 1-g and 0-g environments.

The simplified block diagram for the final prototype can be found in Figure 2-

3, where dashed lines represent Qwiic connections and solid lines represent soldered connections. The final wiring diagram is represented in Figure 2-4.
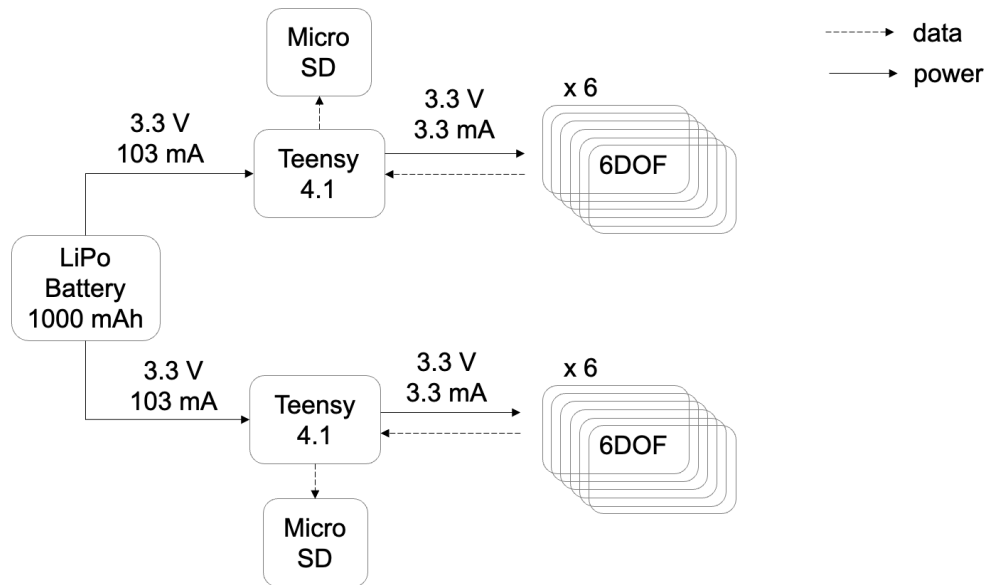
Figure 2-3: Simplified block diagram for the final prototype. Power and data streams are shown with solid and dashed arrows, respectively.
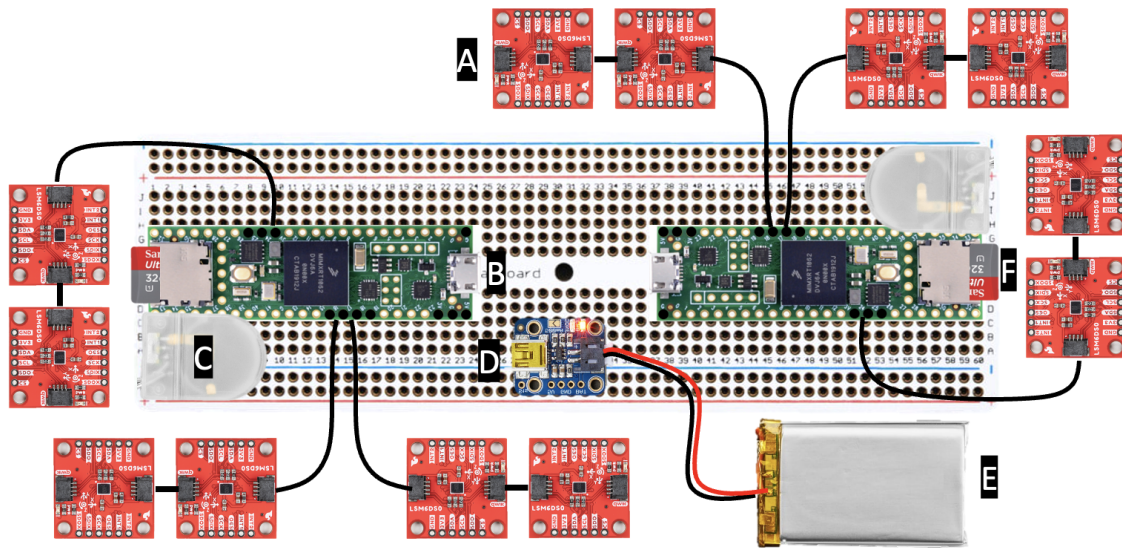

Figure 2-4: Full system wiring diagram of final flight-version system. Components are labeled from the top going counterclockwise. A (6DOF accelerometers); B (Teensy 4.1 microcontrollers); C (coin cell battery for RTC); D(battery backpack for LiPo recharging and supplying power); E (LiPo battery); F (microSD card).

2.6 Garment Integration and Ergonomics

Each of the two microcontrollers connected to six accelerometers. Each of the three I2C channels on each microcontroller accommodates two accelerometers per Figure 2-4.

Hand-sewing was the only viable method of attaching components that provided the option of reattachment since alternatives such as fabric glue were permanent. The placement of the sensors was not possible via machine-sewing; the garment was a tight elastic tube and not a flat surface, so it would not have been feasible to only sew on one side of the garment with a standard sewing machine. Sewing allowed for minute adjustments in the tension and placement of the wires after trying on the garment. Due to the flexibility offered by sewing, the sewn sensors could remain attached while the microcontroller systems were updated between the initial and final prototypes. The available Qwiic wire lengths (50 cm, 200 cm, and 500 cm) constrained the design. The connections between the sensors and between the sensors to the microcontroller both relied on these Qwiic connector wires. For each microcontroller, there were three sets of two accelerometers in series. Placement of sensors with respect to the microcontrollers was carefully considered to ensure no wires crossed or caused a tangle risk. The prototype was built to fit a 165 cm, 50 kg female flyer.
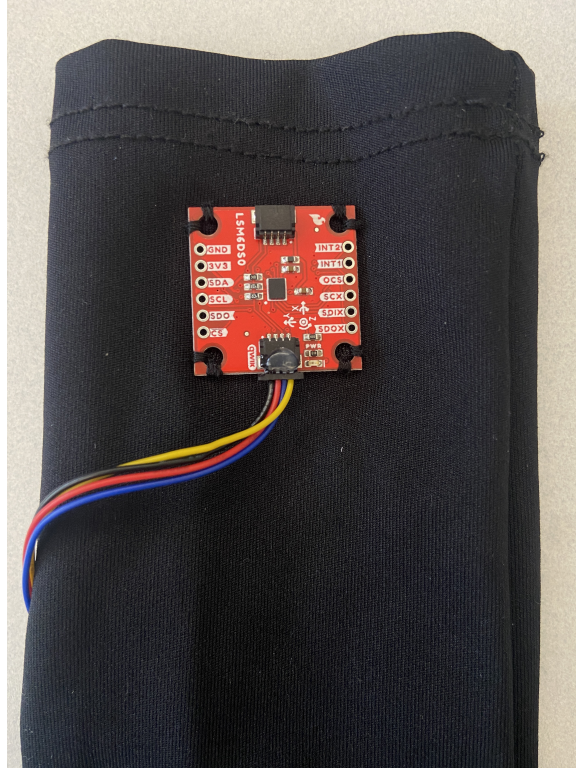
Figure 2-5: Hand-sewn detail of accelerometer attached to the garment at the wrist.

The microcontrollers both connected to a solderable breadboard, which sat atop the chest. This breadboard position minimized the number of wire length adjustments and optimized ergonomics. The left microcontroller corresponded to three I2C wire paths: two shoulders, left elbow and wrist, left knee and ankle. The right microcontroller corresponded to the remaining three I2C wire paths: two hips, right elbow and wrist, right knee and ankle. Several wire paths were adjusted, since wires that were too long caused tangle risks and wires that were too short resulted in broken connections with movement. The sensors were sewn on the headward side of joints and dorsal to the body (e.g. on the dorsal side of the forearm above the wrist or on the dorsal side of the thigh above the patella) to avoid interference with the joints during movements. Each of the sensors had four solder holes in each corner, which we used to sew three passes on each external side, as shown in Figure 2-5. The breadboard was secured in a similar fashion with the four corners sewn in as shown
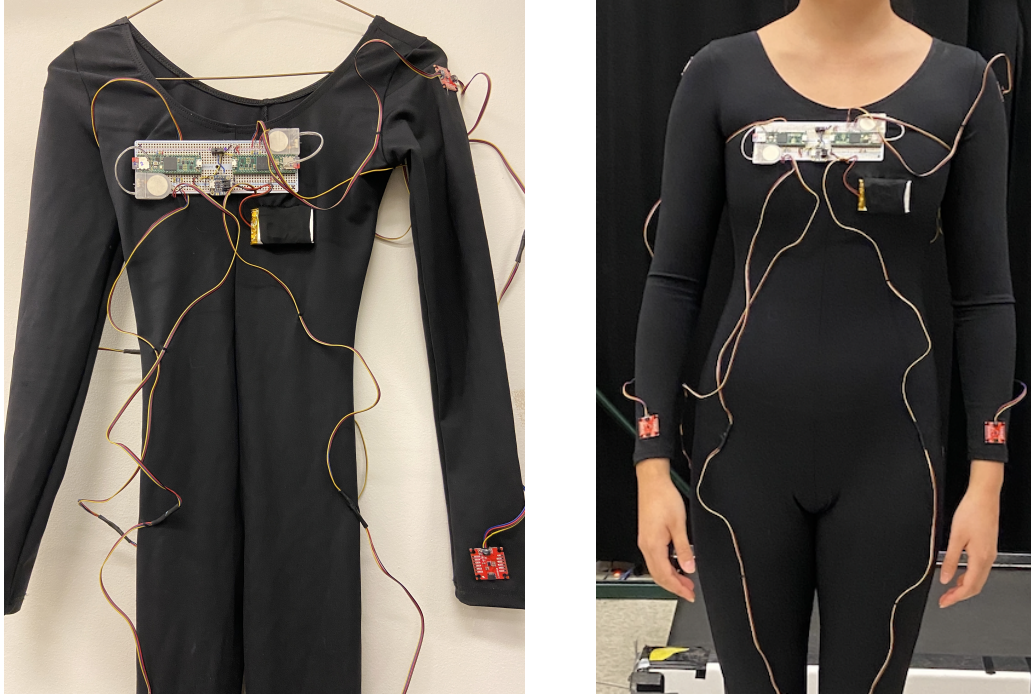
(a) Final prototype garment close up.   (b) Final prototype garment on-body.

Figure 2-6: Final prototype garment.

in Figure 2-6, with the garment stretched underneath so it would be flush when put on. The electronics and wiring were left exposed throughout the prototyping process since LEDs on each sensor served as visual indications for electrical connections. The microcontrollers were left exposed to accommodate manual access on flight day. Zero Gravity Corp. required their flight suit to be worn on top of the garment, so the decision to leave the electronics exposed saved time and did not increase risk to the user or system.

Range of motion tests were conducted to choose appropriate wire lengths for the system. For any wire, we chose the maximum extended range of motion for that particular wire and set that as our wire length. A midpoint was chosen where the wire was secured to the garment with thread loops in order to create friction, but not attached so the wire was able to slide back and forth as needed. The wrist-elbow and knee-ankle wires were wrapped around the forearm and calf respectively to reduce excess wire. Wires that needed modification were spliced and wrapped with heat

shrink. The movements at the full range of motion were again conducted to ensure there was no excessive slack (more than 10 cm hanging from the body) or insufficient slack (wire tugging at the full range of motion). Once the wire lengths were verified, the connectors were secured with hot glue to ensure retention during movement.

2.7   Lessons Learned

The build process was very time-consuming. While unforeseen developments often arise in research, the process was more efficient whenever we followed a strict plan. Creating a wiring diagram, a breadboard prototype, then a detailed soldering plan were crucial steps to our timely delivery of the final garment. Sometimes, we strayed from the plan as we were caught up in creating the tangible end product, but we almost always had to backtrack and lost any short-lived progress. Proceeding from least to most permanent methods of attachment allowed us to backtrack. For example, splicing and attaching the wires before soldering one end to the breadboard allowed us to change wire paths completely or switch out wires without needing to re-solder components.

Although physical ergonomics was a priority throughout the design and build process, it was difficult to ensure comfort and mobility with the COTS components we used. Limited wire lengths, sharp corners, and hard components were challenging to integrate with a soft fabric garment. The vertical profile of the components and attachment methods (i.e. vertical wire plugged into a breadboard) revealed that most electronic components were not designed for end products that required a minimal profile. These limitations encourage us to look for more contemporary methods such as textile-embedded circuitry.

One potential improvement with a future system would be integrating the circuit into the garment with conductive thread. Switching away from fixed-length Qwiic

wires will speed up the build time considerably, even when hand-sewing the circuits. While Qwiic connections were helpful during the prototyping process, the wires posed a tangle risk. The wires were also the main ergonomic consideration, since small alterations in wire paths and lengths created very noticeable changes in comfort and mobility restrictions. The chest-mounted breadboard was the most ergonomic option, but the length of the board created pressure where the middle of the board was in contact with the wearer. Eliminating the wires and the breadboard by introducing conductive threading and other 'soft electronics' such as conformable and elastic circuits would increase the comfort of the wearable system.

Chapter 3

Methods

In this chapter we describe how our research questions and corresponding hypotheses lead into an experimental design. We detail the data analysis approach to processing the raw data, transforming linear acceleration to the Fluidity Index (FI), a full mathematical derivation of FI, the statistical analysis plan including non-parametric alternatives, and a power analysis.

3.1 Research Questions and Hypotheses

Our research questions are

1. How does fluidity change upon introduction to microgravity?
2. How does fluidity change throughout short-duration microgravity exposure?

which will help us address the adaptability and the capability portions of proprioceptive competence (Definition 1.2.1), respectively.

Our corresponding hypotheses are

1. Fluidity decreases upon introduction to microgravity as compared to ground measurements.
2. Fluidity increases over time during microgravity exposure.

3.2 Experimental Design

To test our hypotheses, we created comparable tasks for the ground (1-g) and microgravity (0-g) environments. To investigate proprioceptive competence as provided by Definition 1.2.1, we need to quantify adaptability from a familiar to a novel environment, and capability in that novel environment. We chose "translation" as the task across ground and flight conditions, since it could be adapted across different gravity levels and provided full body movement. Ground translation comprised of a walking task to a target on the wall directly in front. The flight counterpart was a traverse from a supine position on the plane floor to a target on the bulkhead wall. The translation distances were approximately equal and both tasks required a target touch to signal end of traverse.

The human participant study protocols mentioned in this section adhere to the guidelines set by MIT's Committee on the Use of Humans as Experimental Subjects (COUHES). Supporting COUHES documentation for this study can be found in Appendix C. Due to the course constraints and the limited flyer seats for the parabolic flight, we were able to have one participant ($n = 1$) and 20 trials ($N = 20$) for this pilot study. Note the usage of lower and uppercase letters to denote participant and trials.

3.2.1 Ground Experiments

For the ground portion of the experiment, the participant was asked to rise from a sitting position from a wooden chair, traverse a distance of 4 meters, and touch the surface in front of them to signal the end of the traverse. Acceleration data was recorded from the sitting position until the end of the traverse. This translation task was repeated 20 times to allow for a margin of error. The setup is shown in Figure 3-1.

3.2.2 Flight Experiments

For the flight portion of the experiment, the participant was asked to rise from a supine position on the floor, traverse to a target, and touch the target to indicate the end of the traverse. The target was located on the wall at the end of the plane, and the traverse started at the floor of the plane. The total traverse distance is the hypotenuse created from the height of the target on the wall and the horizontal distance from the floor position to the wall. At 3.6 meters, the total traverse distance was the maximum allowed based on the flight setup. Acceleration data was recorded from the supine position at the beginning of the microgravity parabola until the end of the traverse. There were 13 opportunities for recording in microgravity (see Table 2.2) and parabolas 6, 7, 8, 9, 12, 13, 14, 15, 16, and 17 were recorded for a total of 10 parabolas. Traverses were scheduled in each of the three sections of flight. Operational factors including the uneven distribution of microgravity parabolas and photography opportunities constrained the amount and spread of the data that could be obtained. Additionally, the flight manifest was changed during the flight to substitute two microgravity parabolas for additional lunar parabolas for other on-board research.

(a) Ground experimental task   (b) Flight experimental task

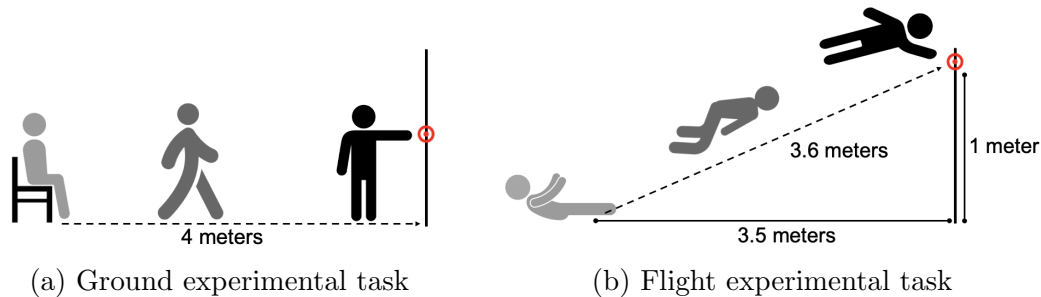Figure 3-1: For the ground experiment, participants started in a seated position on a chair, then walked a distance of 4 meters, and touched the surface in front of them to conclude the traverse. For the flight experiment, participants started in a supine position on the plane floor, then traversed a distance of 3.6 meters, and touched the corner between the plane ceiling and the bulkhead wall to conclude the traverse.

3.3 Data Analysis Approach

3.3.1 Data Processing

There were two `.txt` data files for each experimental condition (ground, flight), one corresponding to accelerometers 1-6 and the other to accelerometers 7-12. We also collected static data for 2 hours.

We translated the time column into seconds. The data files from the two micro-controllers did not start data collection at the same time, so datapoints from both microcontrollers were adjusted to use the earliest time recorded across both data files as a zero reference. The remaining values were divided by 10,000 to obtain the true values (see Section 2.4 for rationale of the multiplier).

Then, we restructed this data file into two `struct` variables in MATLAB, following the `struct_name.Trial_#.IMU_#.variable` format, where the `variable` corresponds to acceleration or rotation in the x, y, or z direction.

3.3.2 Jerk and Fluidity Calculations

We first calculate the magnitude of acceleration from the components of acceleration as

$$a = \sqrt{a_x^2 + a_y^2 + a_z^2}$$

where a_x, a_y, and a_z are the x, y, and z components of acceleration. Here, a is a time-varying vector for each trial and accelerometer combination.

Jerk is defined by

$$j = \frac{da}{dt} \tag{3.1}$$

where a is acceleration in g's and t is time in seconds. Here, j is a time-varying vector for each trial and accelerometer pair.

Previously, we introduced Piana et al.'s definition of fluidity. They provided the

equation below:

$$\text{FI} = \frac{1}{\int (j_i + 1)dt}$$

where FI is a numerical index that describes the fluidity of a movement over the entirety of the movement. Although details were not provided in the paper, we speculate the jerk (j_i) is the magnitude of the jerk and the 1 is added to the integrand to keep the denominator of the fraction positive and non-zero.

Two limitations exist with the definition. The index is not bounded, and possible values for FI exist between $(0, \infty)$ dependent on the duration of the movement. The index also "penalizes" movements with a longer time duration, as the integral is over time. For a movement with a longer time-duration, the Fluidity Index will be smaller than that with a smaller duration even if the average jerk, smoothness, and movement quality of the movements are the same. Or, short jerky movements can have the same FI as longer smooth movements.

The ground and flight data are not equal in time; ground traverses were executed in about half the time as flight traverses. We also required a 'normalized' index from $(0, 1]$ to have a defined and constrained range for cross-comparison. To adapt this jerk-based definition for our needs, we considered two approaches. For both, we start with a non-negative time-varying vector of jerk,

$$|j_i| = < |j_1|, |j_2|, \cdots, |j_n| >$$

Approach 1 – Arithmetic Mean
Find the time-varying Fluidity Vector such that

$$FV = < \frac{1}{|j_1| + 1}, \frac{1}{|j_2| + 1}, \cdots, \frac{1}{|j_n| + 1} > \tag{3.2}$$

Notice here that the reciprocals are taken for every time step i and not integrated

in time, which constrains the range of values from $(0, 1]$.

The modified Fluidity Index is then

$$FI_{AM} = \frac{\sum FV}{n} \tag{3.3}$$

which is the arithmetic mean of the Fluidity Vector. This value can be interpreted as the average of fluidity values over the whole movement, where fluidity is inversely proportional to jerk.

Approach 2 – Harmonic Mean

The second approach starts with the average of the modified jerk vector for the Jerk Index, where 1 is added to prevent dividing by 0 in the Fluidity Index definition later.

$$JI = \frac{\sum(|j_i| + 1)}{n} \tag{3.4}$$

The Fluidity Index is then the reciprocal of JI

$$FI_{HM} = \frac{n}{\sum(|j_i| + 1)} \tag{3.5}$$

and this definition is the harmonic mean of the Fluidity Vector (Equation 3.2). This value can be interpreted as the reciprocal of the average jerk values over the movement.

Both definitions utilize an averaging function, a summation, and an inversely proportional relationship between fluidity and jerk. Both definitions are adequate to address the research question, as taking an average of jerk or fluidity allow us to ultimately examine the same fundamental ideas. However, the subtle difference in the order of operations make these two definitions mathematically and numerically different. This is known as the HM-AM inequality, where 0≤HM≤AM for all combinations of numbers. For a conservative estimate of fluidity, we opt to take the harmonic mean definition offered in Equation 3.5.

3.3.3   Statistical Analysis Plan

In order to address the two hypotheses, we will conduct two statistical analyses. The data will be tested for violations of normality through a Kolmogorov-Smirnov test and homoscedasticity (equal variances) through Bartlett's test (or Levene's test if data is non-normal), and statistical test modifications should those requirements not be met will be presented. We acknowledge that with $n = 1$, all inferences from the statistical tests can only be used to assess differences in this participant under different conditions, not the population as a whole.

Adaptability Analysis

There is only one experimental participant, so this is a one-way repeated measures study analyzing the effect of gravitational environment on joint fluidity. The independent variable here is the gravitational environment with two factor levels (Earth gravity, microgravity). The experimental participant completed 10 trials in each level. The dependent variable is joint fluidity, which is a continuous ratio variable with 0 corresponding to jerk approaching infinity.

Table 3.1: Experimental setup for the adaptability statistical analysis. There is one independent variable with two factor levels and 10 trials each level for a total of $N = 20$.

Earth gravity	Microgravity
$N_1 = 10$	$N_2 = 10$

The standard test for a comparison between two dependent data sets is a dependent t-test. The assumptions of a dependent or paired t-test are

- Dependent variable is continuous

- Independent variable is categorical and related

- No significant outliers in the dependent variables

- Dependent variables follow a normal distribution

The numerical values of the independent variable have a ceiling (human movement is limited), so the data are likely non-normally distributed. The non-parametric version of the dependent t-test is the Wilcoxon two-tailed signed rank test. The Wilcoxon signed rank test tests for differences in the median (Θ) differences between the two groups, where

$$H_0 : \Theta_d = 0$$

$$H_a : \Theta_d \neq 0$$

Capability Analysis

This is a one-way repeated measures study analyzing the effect of time in microgravity on joint fluidity. The independent variable here is time spent in microgravity, with three factor levels (first parabolic section, second parabolic section, third parabolic section). There were 4, 4, and 2 trials conducted in each factor, respectively. The dependent variable is joint fluidity.

Table 3.2: Experimental setup for the capability statistical analysis. There is one independent variable with three factor levels; there are 4, 4, and 2 trials per level for a total of $N = 10$.

1st parabolic section	2nd parabolic section	3rd parabolic section
$N_1 = 4$	$N_2 = 4$	$N_3 = 2$

The test we elect for comparison between 3+ dependent groups is the one-way analysis of variance (ANOVA). We can opt to use an ANOVA instead of a repeated measures ANOVA as $n = 1$. However, ANOVA tests assume equal variances and normally distributed data. If the data violate the normality assumption, we can

pursue the non-parametric version of a one-way ANOVA, which is the Kruskal-Wallis test. The Kruskal-Wallis test provides information about whether datasets come from the same distributions, such that

H_0 : Each group comes from the same distribution

H_a : At least one group comes from a different distribution than the other(s)

After the ANOVA model is fitted, we will conduct an analysis of the residuals. If the model fit is appropriate, we expect the residuals to be normally distributed around 0 and all three factor levels should exhibit equal variances with no outliers. We expect visual inspection for normality and homoscedasticity may be difficult due to the small size of the data set. We will follow with formal tests if necessary. Note that we will not conduct any post-hoc fit checks for a Kruskal-Wallis test since it does not provide a linear model with predicted values and corresponding residuals.

3.3.4   Effect Size & Power Analysis

We expected to see a very small effect size (estimated Cohen's d ≈ 0.2, where < 0.2 is small, ≈ 0.5 is moderate, and > 0.8 is large) and power ($\beta < 0.5$) for this study due to the uncontrolled effects between the experimental setup and the operational environment. Space and parabolic analog studies also share the same limitations for small sample sizes. Two studies by Papaxanthis in 1998 had $n = 2$ for a pointing experiment, in 2005 had $n = 5$ for a similar experiment, and Castellato et al. in 2017 had $n = 3$ for a whole body experiment [8][28][29]. The last was done on a spaceflight mission while the other two were through parabolic flights. These small sample sizes are consistent for human spaceflight studies requiring access to microgravity. Constraints of the experimental paradigm as a course project contributed to the small participant number. Limited iterations, manufacturing time, and budget consequently limited the number of garment systems that could be made. Flyer seats

were also limited to one flyer per project. Since all flyers had their own projects, participating in our experiment was unfavorable as it distracted them from their own research, especially considering that the participants would not have been monetarily compensated due to budget limitations. The need for anthropometric personalization of the garment system to maintain a conformal fit thereby preserving accelerometer signal integrity further added complexity to the already constrained manufacturing timeline and budget. For these reasons, this experiment does not have any additional participants and is likely to be underpowered with $n = 1$ and $N = 20$.

Calculating effect size a posteriori, we get a Cohen's $d = 0.87$. Adjusting for the small n, we also get Hedge's $g = 0.83$. Both of these are large (> 0.8) and higher than expected. However, note that effect sizes of studies with small sample sizes ($N < 30$) are less accurate [36]. Each ground and flight data vector had 10 values. Each value represents the whole-body Fluidity Index for each trial, averaged over all accelerometers. Means and variances were calculated from these whole body values, with variances propagated from averaging over accelerometers and covariances between trials (down each column in Table 3.3).

Table 3.3: Fluidity Indices for accelerometer/trial pairs. Each FI value is the time-averaged harmonic mean over each trial and accelerometer pair. Values are then averaged over all accelerometers for a 'whole body' FI mean and variance representing each trial. Mean values are used in comparison between ground and flight data, and variances are propagated forward for effect size calculations.

	Trial 1	Trial 2	$\cdots$	Trial 10
Accel 1	$FI_{1,1}$	$FI_{1,2}$	$\cdots$	$FI_{1,10}$
Accel 2	$FI_{2,1}$	$FI_{2,2}$	$\cdots$	$FI_{2,10}$
$\cdots$	$\cdots$	$\cdots$	$\cdots$	$\cdots$
Accel 12	$FI_{12,1}$	$FI_{12,2}$	$\cdots$	$FI_{12,10}$
$\downarrow$	$\downarrow$	$\downarrow$	$\downarrow$	$\downarrow$
Whole body	μ_1, σ_1^2	μ_2, σ_2^2	$\cdots$	μ_{10}, σ_{10}^2

At n = 20 (df = 18) for a t-test for the adaptability analysis (between ground and flight), we can estimate power using $\alpha = 0.05$ ($z_{1-\alpha/2} = 2.101$) for a $\beta = 0.45$ from the t-table, which is underpowered as we expected.

Constraints on Generality

This statement aims to discuss constraints on the generality of these results. With $n = 1$, any trends or results we see are limited to that person; we cannot make conclusions for the general population without more data. While recognizing the limitations of a pilot study, we also discuss some factors that may contribute to the potential generality in support of future studies and/or applications of this framework. The study participant is a parabolic flight novice, which is similar to the target population that participates in commercial suborbital flights and parabolic flights. The participant has had training in classical ballet, which has been speculated to aid with proprioception in microgravity [11]. However, as a non-professional dancer, we believe the participant is moderately advantaged at most and do not expect significant deviation from the average person in terms of proprioceptive ability. Although on the younger side, this participant is within the age range of eligible passengers for a commercial flight. While generality limitations do exist for an underpowered study, we have determined that the participant is an adequate example of someone we would study from the target population.

Chapter 4

Results and Discussion

In this chapter, we discuss the steps taken to process raw acceleration data provided by the sensors to whole-body Fluidity Index (FI) values. We discuss outlier determination, the downsampling process, and show examples of time and frequency-domain data. Then, we provide results from the statistical analysis with a detailed discussion on the results and their limitations. The code used to perform these processes can be found in Appendix D.

4.1   Data Cleaning

We conducted a static test with all systems on and recording for two hours. However, upon post-processing, it was revealed that the sensor capabilities did not allow for accurate measurements of near-zero values of acceleration. The noise present in the static data rendered it unusable for analysis.

The ground experiment (walking traverse) was repeated for 20 trials. In one trial, the participant did not traverse with the same posture present in all other trials. Their head was tilted downward with the gaze to the floor immediately after rising from the seated position and kept the gaze on the floor for half the traverse. For comparison, the participant was looking at the target during the traverse for all other

trials. This deviation did not technically violate the experimental protocols, so we noted the qualitative difference here and accepted it as a valid trial. There are 20 ground trials available for random pairing to the flight data. Due to the excess number of ground trials in comparison to flight trials, we paired each flight parabola with the corresponding ground trial number for analysis.

An example of the original signal can be found in Figure 4-1 where acceleration data from a trial and accelerometer pair were plotted. The Fast Fourier Transform (FFT) plots from the original acceleration data were also plotted. The frequency content of the ground data mostly fell in the 0-20 Hz range, with the majority contained below 15 Hz. In comparison to ground data, more frequency content fell in the 20-50 Hz range for flight data, with the majority of the signal contained below 20 Hz. The frequency contents shown here are consistent with literature, which report human motion frequency is limited within 20 Hz, with 99% of gait energy contained within 15 Hz [1][18]. Note that the upper end is capped by 50 Hz as that is the Nyquist frequency of the original signal at 100 Hz.
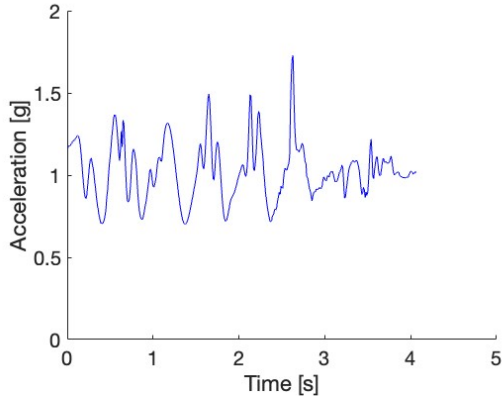
(a) Ground acceleration data at original frequency of 100 Hz
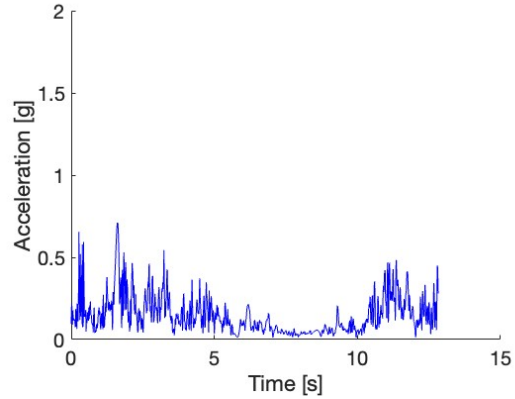
(b) Flight acceleration data at original frequency of 100 Hz
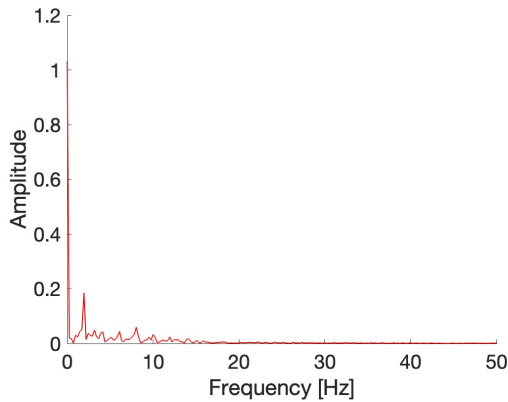
(c) Ground FFT at original frequency of 100 Hz
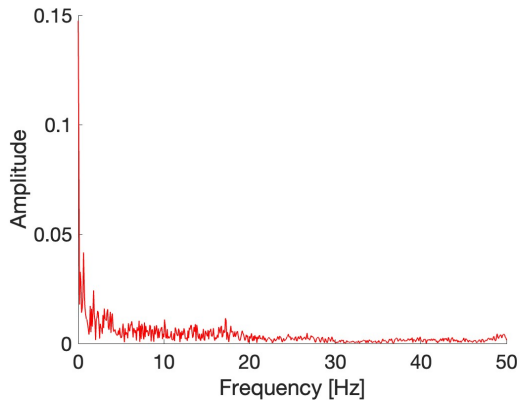
(d) Flight FFT at original frequency of 100 Hz

Figure 4-1: Original frequency data for sample ground and flight acceleration from an example trial and accelerometer pair. The ground data was taken with the Earth 1-g reference, which causes the discrepancy in the ground and flight acceleration values.

The ground acceleration in Figure 4-1 is centered around 1 g due to the Earth's gravitation field. The range of acceleration and the cyclic pattern matches literature on gait [40][15]. This allows us to validate the acceleration data. While we were unable to determine the source of noise in the flight data, we constrained the data within 0-20 Hz for analysis, again noting that human activity falls within this range [1][18]. To avoid aliasing from downsampling directly, we placed a low-pass filter on the data at 40 Hz before performing a spline interpolation. The spline option was chosen to maintain continuity in the derivatives. The downsampled frequency and

corresponding FFT plots of an example trial and accelerometer pair can be found in Figure 4-2. For each trial and accelerometer pair, the acceleration data were then transformed into jerk and FI. The FI values were averaged within each trial across all accelerometers for a whole-body FI.

(a) Ground acceleration at 40 Hz

(b) Flight acceleration data at 40 Hz

(c) Ground FFT at 40 Hz

(d) Flight FFT at 40 Hz
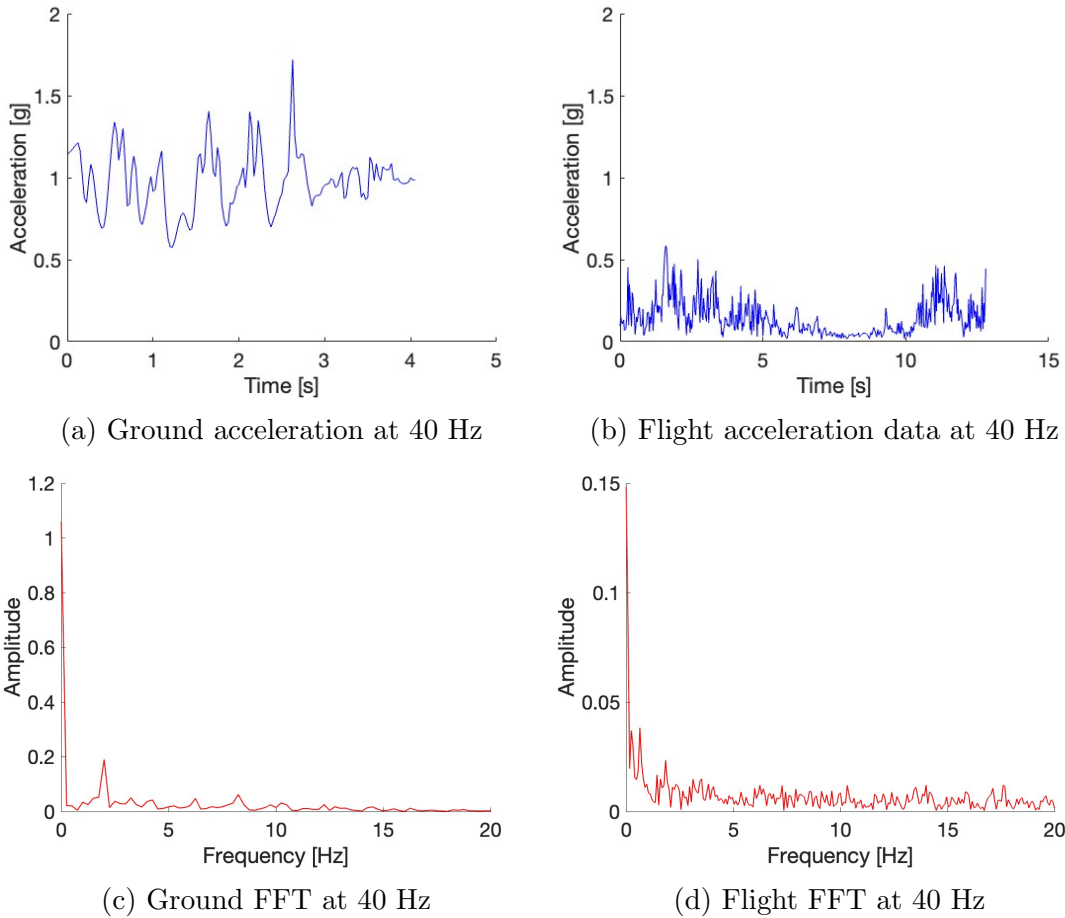
Figure 4-2: Downsampled (40 Hz) data for ground and flight acceleration from an example trial and accelerometer pair. The ground data was taken with the Earth 1-g reference, which causes the discrepancy in the ground and flight acceleration values.

4.2 Statistical Analysis

To assess normality of the data set, we ran the Kolmogorov-Smirnov (KS) test for a standard normal distribution on the ground and flight whole-body FI values. For both ground ($h = 1, \alpha = 0.05, p < 0.0001$) and flight ($h = 1, \alpha = 0.05, p < 0.0001$),

we conclude that there is evidence to reject the null hypothesis that these data come from the normal distribution. The data violates the normality assumption and we were not able to transform the data set to normalize it. Therefore, we will elect to use non-parametric statistics.

To test for equal variances, we used Levene's Test, which is a modification of Bartlett's test that is less sensitive to departures from normality. We used the Levene Absolute option, which tests for homogeneity of variances by assessing the absolute deviations of the observations from the group mean, with the null hypothesis being that the groups being tested have equal variances. Comparing the variances between ground and flight whole-body FI ($h = 0, \alpha = 0.05, p = 0.234$), Levene's test fails to reject the null hypothesis, and we can conclude that variances are equal in ground and flight data.

4.2.1 Adaptability – Initial Response

Averaging the FI values for all accelerometers within each run, we obtain means and variances within trials. Mean joint FI values are plotted for each run of ground and flight data with variances as error bars in Figure 4-3.

The data violated the normality assumption. We used the Wilcoxon two-tailed signed rank test for dependent samples, which is the non-parametric alternative to the dependent t-test. Note that we are using a two-tailed test for a more conservative estimate since we have no prior evidence to elicit the use of a one-tailed test even though our hypothesis is phrased for a one-tailed test. Comparing the medians of ground and flight whole-body FI values at $\alpha = 0.05$, we get the Wilcoxon test statistic W = 5 (df = 19, $p = 0.0195$). We have evidence to reject the null hypothesis at a 5% significance level that the medians of the ground and flight whole-body FI values are significantly different from each other. Contrary to our hypothesis, "*fluidity decreases upon introduction to microgravity as compared to ground measurements*", we saw an

increased median fluidity for the flight condition ($FI_D = 0.76$) compared to ground ($FI_D = 0.67$) as visually represented in Figure 4-4. The error bars are propagated variances from the sum of the variance within each run and the covariances between runs.

Recalling that one of the trials in the ground experiment was altered; the participant did not traverse with the same posture as in all other trials. The participant's gaze was kept to the floor for half of trial 14, and corresponded to a lowered FI with greater variance as compared to other trials with equal posture (gaze straight ahead).
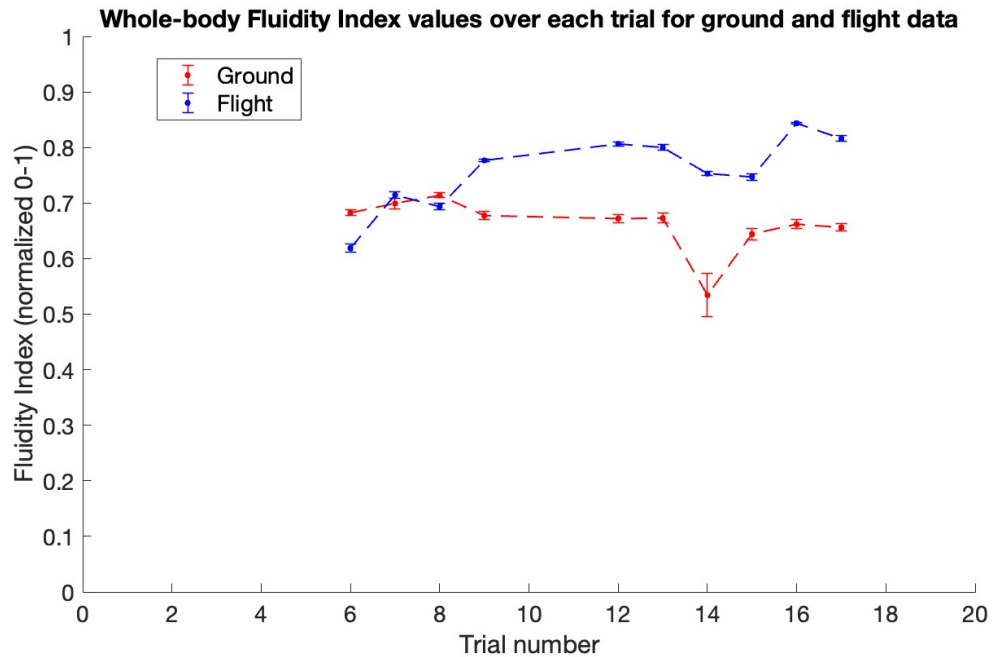
Figure 4-3: Whole-body Fluidity Index values (averaged over all accelerometers) for each trial are plotted for ground and flight conditions. Mean averaged joint FI values over each trial are plotted with variance error bars. Dashed lines are used for ground/flight grouping, but no data exists between the trials.
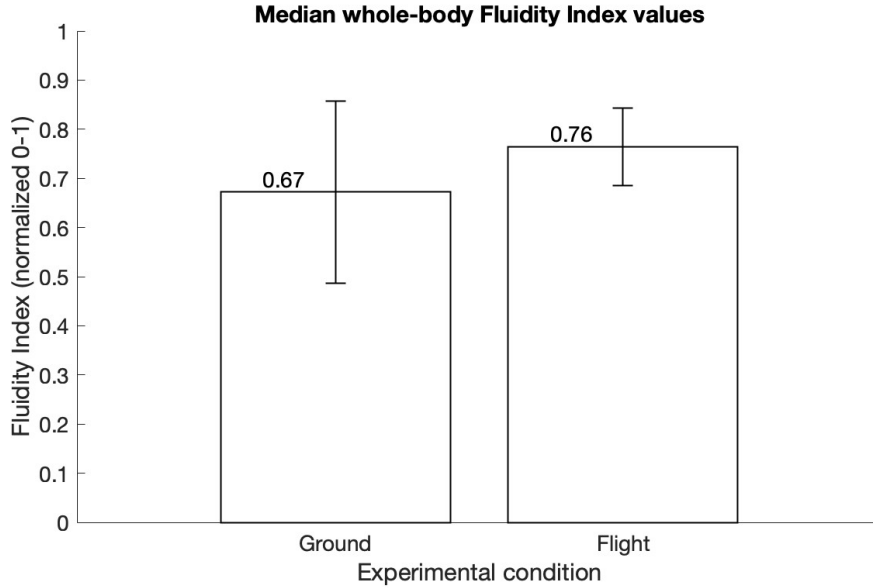
Figure 4-4: Median whole-body FI values over all trials for ground and flight conditions. Error bars are propagated variances from summed variances within run and covariances between trials.

4.2.2 Capability – Exposure Response

For the capability assessment, we are interested in the differences between the fluidity of movements in the first, second, and third parabolic sections. This corresponds to parabolas 6-9, parabolas 12-15, and parabolas 16-17.

We used the non-parametric alternative to the one-way ANOVA, the Kruskal-Wallis test. The Kruskal-Wallis one-way ANOVA results are replicated in Table 4.1, tested at a significance level of 5%. Testing for significant differences in the fluidity values from three flight sections, we get $\chi^2(2, N = 10) = 6.33$, $p = 0.0423$. We have evidence to reject the null hypothesis that the groups under test come from the same distribution, and we conclude there is at least one section that is significantly different from the other section(s).

Table 4.1: Kruskal-Wallis one-way ANOVA results comparing fluidity values from parabolas in three different sections to understand longitudinal effects. The test was conducted at $\alpha = 0.05$ and * indicates significance.

Source	SS	df	MS	Chi-sq	Prob > Chi-sq
Groups	58	2	29	6.33	0.0423*
Error	24.5	7	3.5		
Total	82.5	9			

We conducted pairwise comparisons for all section combinations with the Bonferroni correction. Results of the pairwise comparisons are available in Table 4.2. Section 1 and 3 had a χ^2-statistic difference of 6.5 with $p = 0.0395$, providing sufficient evidence to reject the null hypothesis that sections 1 and 3 come from the same distribution. Therefore, we can conclude that sections 1 and 3 are significantly different ($\alpha = 0.05/3$). There was insufficient evidence to reject the null hypothesis for the other pairwise comparisons, and we accept that sections 1 and 2, as well as sections 2 and 3, are not significantly different.

Table 4.2: Summary of the pairwise comparison test for whole-body FI values from flight sections with the Bonferroni correction at an original significance of $\alpha = 0.05$, where * indicates significance. Mean rank statistics are from the Kruskal-Wallis test.

Section	Section	Mean rank difference	p-value
1	2	3	0.483
2	3	3.5	0.5458
1	3	6.5	0.0395*

4.3 Discussion

Recall our research questions

1. How does fluidity change upon introduction to microgravity?

2. How does fluidity change throughout short-duration microgravity exposure?

and hypotheses

1. Fluidity decreases upon introduction to microgravity as compared to ground measurements.

2. Fluidity increases over time during microgravity exposure.

We found a statistically significant difference between the ground and flight whole-body FI values (W = 5, df = 19, $\alpha = 0.05$, $p = 0.0195$). This result suggests that joint fluidity was higher in microgravity trials than ground trials when averaged over the whole body. This is the opposite of our original hypothesis and we see that fluidity increases upon introduction to microgravity as compared to ground measurements. From Figure 4-4, we see that $\Delta D_{FI} = 0.08$ between ground and flight conditions, which is about a 12% increase with respect to baseline ground FI. Referencing Figure 4-4, we see that the variance from the ground data exceeds the range of values from the flight data, which indicate that any difference we see may be due to individual or experimental variation. From the result of our statistical analysis, **one explanation is that the fluidity of constrained and goal-oriented traverses are not adversely affected, or could be increased in microgravity.** Goal-oriented traverses could provide the participant with a focus point and consequently prevent the flailing that first-time participants resort to during microgravity exposure. Further experimentation with a broader set of constrained, goal-oriented, dynamic movements and an increased participant pool would contribute power to this explanation.

We found statistically significant differences in whole-body FI values between section 1 and section 3 of the parabolic flight ($\Delta \chi^2(2, N = 10) = 6.5$, $\alpha = 0.05/3$, $p = 0.0395$), which means that joint fluidity during the traverses of the last parabolic section was higher than that of the first section. While whole-body FI values are increasing from section 1 ($\mu_1 = 0.6593$, $D_1 = 0.6611$) through section 2 ($\mu_2 = 0.7382$, $D_2 = 0.7387$) to section 3 ($\mu_3 = 0.7924$, $D_3 = 0.7924$), the differences between sections 1 & 2 and sections 2 & 3 were not statistically significant. While we can't

conclude relationships between sections 1 & 2 or sections 2 & 3, the movements during the last section were more fluid than those during the first section. We are able to partially support our original hypothesis that fluidity increases over time during microgravity exposure. Other studies corroborate the adaptation process observed during the length of a parabolic flight for hand kinematics and push-off force, respectively [28][39]. While there was a consistent increase in FI over each section, we do not see continuous increases from parabola to parabola, indicating that sustained adaptation was not reached [6]. **We have evidence supporting the presence of a proprioceptive adaptation over the duration of a parabolic flight, but the data suggest sustained proprioceptive adaptation as measured by fluidity requires longer or more continuous exposure to microgravity.**

We observed a lowered FI and increase variance in ground trial 14, which was performed with altered posture, as compared to the other trials. While not part of our formal analysis, this interesting and unexpected result suggests that the FI metric was able to capture deviations of qualitative fluidity and whole-body dynamics.

This pilot study had several limitations that should be considered along with the results. The single participant limits any statistically significant trends or conclusions to be within the individual exposed to this gravitational environment factor, not to any general populations. First exposure to the reduced gravity environment was also not distinct, as three Martian and two Lunar gravity-level parabolas preceded the microgravity parabolas. The exposure to the microgravity environment was also not continuous, as the flight profile altered between 20-second periods of microgravity and periods of hypergravity (1.8 g). The participant also applied a transdermal scopolamine patch prior to the parabolic flight to prevent motion sickness. Lastly, a limitation of the experimental paradigm may be that the participant also designed the experiment. While multiple measures were implemented to prevent bias, we recognize this as a limitation in the experiment due to the course structure. We constrained

the tasks to a traverse and did not arbitrarily observe free motion, which provided a structured protocol that could be generalized to other participants. Additionally, the participant was completely untrained. As a novice, we would not expect them to have had the control or prior knowledge to bias the outcome.

Chapter 5

Conclusion

To conclude, we summarize our research contributions and discuss future opportunities for expansion on this work.

We introduced the terminology 'proprioceptive competence' as a functional construct for the continual adaptation of the proprioceptive system in novel gravity environments. Our fluidity framework uses fluidity as a metric for proprioceptive competence for the first time in the microgravity context. We improve upon the definition of fluidity used in other experiments by providing a duration-agnostic and normalized metric that relies on minimum jerk theory [13][31]. Our work is situated in the scientific gap for proprioceptive and neurovestibular research, especially in whole-body, functional, and dynamic movements [5].

Building off of complementary work, we developed a medium-frequency, self-sufficient wearable motion capture system for deployment in parabolic flight. We established two translation tasks as analogous experimental protocols in Earth-gravity and microgravity. After conducting experimental trials in both gravitational conditions, we obtained significant differences between the ground and flight median whole-body fluidity values. This result suggests fluidity may increase upon introduction to microgravity, against our original hypothesis. Throughout microgravity

exposure, we observed increases in whole-body fluidity between the flight sections, but not consistently within sections. This suggests proprioceptive adaptation throughout the length of the parabolic flight, but not full adaptation.

Limitations of this work include the small sample size ($n = 1, N = 20$), which constrains the generality of our results. However, we believe this pilot study has provided novel research insights into physiological adaptation in microgravity. We demonstrated the utilization of a transdisciplinary framework (the Fluidity Framework) to quantify whole-body movement quality in microgravity. We detected correlation between FI and qualitative fluidity observed during experimentation, specifically deviations from nominal posture, gaze, and continuity of motion. This unexpected finding strengthens our framework of utilizing fluidity to assess proprioceptive ability. We also designed and tested a wearable system capable of capturing whole-body motion in the parabolic flight environment. We hope this work introduces a framework others can adopt and draw inspiration from, as well as a reference source for time-constrained prototyping for parabolic flight deployment.

5.1 Disclosures

Bibliography

[1] E. K. Antonsson and R. W. Mann. The Frequency Content of Gait. *Journal of Biomechanics*, 18:39–47, 1985.

[2] T. Asakura and H. Hagiwara. An Accelerometer-Based Method for Estimating Fluidity in the Sit-to-Walk Task. *J. Phys. Ther. Sci.*, 27:3565–3569, 2015.

[3] A. M. Aurand, J. S. Dufour, and W. S. Marras. Accuracy map of an optical motion capture system with 42 or 21 cameras in a large measurement volume. *Journal of Biomechanics*, pages 237–240, 2017.

[4] N. T. Banerjee, A. J. Baughman, S. Y. Lin, Z. A. Witte, D. M. Klaus, and A. P. Anderson. Development of alternative reality environments for spacecraft habitat design evaluation. *Virtual Reality*, 25(2):399–408, 2021.

[5] J. J. Bloomberg, M. F. Reschke, Clement G. R., Mulavara A. P., and Taylor L. C. Evidence Report: Risk of Impaired Control of Spacecraft/Associated Systems and Decreased Mobility due to Vestibular/Sensorimotor Alterations Associated with Space Flight. *National Aeronautics and Space Administration*, 2015.

[6] O. Bock, I. P. Howard, K. E. Money, and K. E. Arnold. Accuracy of aimed arm movements in changed gravity. *Aviat Space Environ Med*, 63:994–998, November 1992.

[7] A. Camurri and G. Volpe, editors. *Gesture-based communication in human-computer interaction: 5th International Gesture Workshop, GW 2003: Genova, Italy, April 2003: selected revised papers*. Number 2915 in Lecture notes in computer science, Lecture notes in artificial intelligence. Springer, Berlin ; New York, 2004. Meeting Name: Gesture Workshop.

[8] C. Casellato, A. Pedrocchi, and G. Ferrigno. Whole-Body Movements in Long-Term Weightlessness: Hierarchies of the Controlled Variables Are Gravity-Dependent. *Journal of Motor Behavior*, 49(5):568–579, September 2017.

[9] W. Chen, J. G. Chao, X. W. Chen, J. K. Wang, and C. Tan. Quantitative orientation preference and susceptibility to space motion sickness simulated in a virtual reality environment. *Brain Research Bulletin*, 113:17–26, April 2015.

[10] J. L. Coldiron. Crew Escape Systems 21002. In A. Flagan and M. J. Alexander, editors, *Space Flight Operations Contract*. National Aeronautics and Space Administration, 2005.

[11] K. Dubois. Dance and Weightlessness: Dancers' Training and Adaptation Problems in Microgravity. Technical report, 1994.

[12] R. A. Fineman, T. M. McGrath, D. G. Kelty-Stephen, A. F. J. Abercromby, and L. A. Stirling. Objective Metrics Quantifying Fit and Performance in Spacesuit Assemblies. *Aerospace Medicine and Human Performance*, 89(11):985–995, November 2018.

[13] T. Flash and N. Hogan. The coordination of arm movements: An experimentally confirmed mathematical model. *The Journal of Neuroscience*, 5(7):1688–1703, 1985.

[14] O. G. Gazenko, A. M. Gernin, and Egorov A. D. Major medical results of the Salyut-6 Soyuz 18 5-day space flight. *Aviat Space Environ Med*, 54, 1981.

[15] J. M. Hausdorff, C. K. Peng, J. Y. Wei, and A. L. Goldberger. Fractal Analysis of Human Walking Rhythm. In J. M. Winters and Crago P. E., editors, *Biomechanics and Nural Control of Posture and Movement*. Springer-Verlag, New York, 2000.

[16] K. T. Johnson, S. Taylor, S. Fedor, N. Jaques, W. Chen, and R. W. Picard. Vomit Comet Physiology: Autonomic Changes in Novice Flyers. *IEEE*, pages 1172–1176, 2018.

[17] R. S. Johnson, L. F. Dietlein, and C. A. Berry. Biomedical Results of Apollo. *National Aeronautics and Space Administration*, NASA-SP-368, 1975.

[18] D. M. Karantonis, M. R. Narayanan, M. Mathie, N. H. Lovell, and B. G. Celler. Implementation of a Real-Time Human Movement Classifier Using a Triaxial Accelerometer for Ambulatory Monitoring. *IEEE Transactions on Information Technology in Biomedicine*, 10:156–167, 2006.

[19] K. Lee and W. Tang. A fully wireless wearable motion tracking system with 3d human model for gait analysis. *Sensors*, 21(12), June 2021.

[20] R. Lum. A Brief History of Motion Tracking Technology and How it is Used Today, 2019. Accessed on February 22, 2023.

[21] J. L. McKay and L. H. Ting. Optimization of Muscle Activity for Task-Level Goals Predicts Complex Changes in Limb Forces across Biomechanical Contexts. *PLoS Computational Biology*, 8(4):1–17, April 2012.

[22] D. J. Newman, A. R. Amir, and S. M. Beck. Astronaut-Induced Disturbances to the Microgravity Environment of the Mir Space Station. *Journal of Spacecraft and Rockets*, 38(4):578–583, July 2001.

[23] A. W. Nicogossian, C. Leach-Huntoon, and S. L. Pool. *Space Physiology and Medicine.* Lea & Febiger, Philadelphia, PA, 1989.

[24] P. Norsk. Physiological effects of spaceflight – weightlessness: An overview. In L. R. Young and J. P. Sutton, editors, *Encyclopedia of Bioastronautics*, pages 1–9. Springer International Publishing, Cham, Switzerland, 2018.

[25] C. O'Kane. Bezos and his Blue Origin crewmates trained for 14 hours. These are the requirements they had to meet, 2021. Accessed on February 17, 2023.

[26] W. Paloski, C. Oman, J. Bloomberg, M. Reschke, S. Wood, D. Harm, B. Peters, A. Mulavara, J. Locke, and L. Stone. Risk of sensory-motor performance failures affecting vehicle control during space missions: A review of the evidence. *J. Gravit. Physiol*, 15, January 2008.

[27] C. Papaxanthis, T. Pozzo, and J. McIntyre. Arm end point trajectories under normal and micro-gravity environments. *Acta Astronautica*, 43(3):153–161, 1998.

[28] C. Papaxanthis, T. Pozzo, and J. McIntyre. Kinematic and dynamic processes for the control of pointing movements in humans revealed by short-term exposure to microgravity. *Neuroscience*, 135(2):371–383, 2005.

[29] C. Papaxanthis, T. Pozzo, K. E. Popov, and J. McIntyre. Hand trajectories of vertical arm movements in one- G and zero- G environments. *Experimental Brain Research*, 120(4):496–502, May 1998.

[30] S. Piana, P. Alborno, R. Niewiadomski, M. Mancini, G. Volpe, and A. Camurri. Movement fluidity analysis based on performance and perception. In *Proceedings of the 2016 CHI Conference Extended Abstracts on Human Factors in Computing Systems*, CHI EA '16, page 1629–1636, New York, NY, USA, 2016. Association for Computing Machinery.

[31] S. Piana, A. Staglianò, F. Odone, and A. Camurri. Adaptive Body Gesture Representation for Automatic Emotion Recognition. *ACM Trans. Interact. Intell. Syst.*, 6(1), March 2016.

[32] M. F. Reschke, J. M. Krnavek, J. T. Somers, and G. Ford. A brief history of space flight with a comprehensive compendium of vestibular and sensorimotor research conducted across the various flight program. *National Aeronautics and Space Administration*, May 2007.

[33] R. Roll, J. C. Gilhodes, J. P. Roll, K. Popov, O. Charade, and V. Gurfinkel. Proprioceptive information processing in weightlessness. *Experimental Brain Research*, 122(4):393–402, October 1998.

[34] R. D. Seidler and A. P. Mulavara. Sensorimotor Adaptation, Including SMS. In L. R. Young and J. P. Sutton, editors, *Handbook of Bioastronautics*, pages 1–5. Springer International Publishing, Cham, Switzerland, 2020.

[35] M. Shelhamer. Trends in Sensorimotor Research and Countermeasures for Exploration-Class Space Flights. *Frontiers in Systems Neuroscience*, 9, August 2015.

[36] R. Slavin and D. Smith. The Relationship Between Sample Sizes and Effect Sizes in Systematic Reviews in Education. *Educational Evaluation and Policy Analysis*, 31:500–506, 2009.

[37] SparkFun. Teensy 4.1. Accessed on February 02, 2022.

[38] ST Microelectronics. LSM6DSO Datasheet, 2019. Accessed on November 10, 2022.

[39] L. Stirling, K. Willcox, P. Ferguson, and D. Newman. Kinetics and kinematics for translational motions in microgravity during parabolic flight. *Aviation Space and Environmental Medicine*, 80(6):522–531, June 2009.

[40] H. Zhang, W. Xu, C. Xu, H. Li, A. Rathore, C. Song, Z. Yan, D Li, and F. Lin. PDMove: Towards Passive Medication Adherence Monitoring of Parkinson's Disease Using Smartphone-based Gait Assessment. *Proceedings of the ACM on Interactive, Mobile, Wearable and Ubiquitous Technologies*, 3:1–23, 2019.

Appendix A

Tables

Comparison of inertial vs. optical motion capture systems.

Motion Capture Systems

Solution	Advantages	Disadvantages
Inertial	Cheaper	Difficult to visualize
	Does not need line of sight	Requires inertial frame
	Raw data	Noisy
Optical	Extreme accuracy	Expensive
	Portable	Software interface
		Requires clear line of sight

Abbreviated course timeline for project course "Prototyping our Sci-Fi Space Future: Designing & Deploying Projects for Zero Gravity Flights" (MAS.838/16.88)

Date	Deliverable
September 14, 2021	Research idea proposal
October 26, 2021	Preliminary Design Review: Motivation, system design, Concept of Operations, risk matrix and mitigation plan, schedule, budget subsystem demonstration
December 7, 2021	Critical Design Review: Full system design, Concept of Operations, experimental setup, full system demonstration
March 11, 2021	Payload Integration Package for flight provider: Hazards information, battery specifications, flight plan
May 20, 2022	Microgravity flight

Parabolic flight profile

Parabola number	Gravity level
1	Martian
2	Martian
3	Lunar
4	Lunar
5	Lunar
3 minute break	
6	Microgravity
7	Microgravity
8	Microgravity
9	Microgravity
10	Microgravity
10 minute break	
11	Microgravity
12	Microgravity
13	Microgravity
14	Microgravity
15	Microgravity
3 minute break	
16	Microgravity
17	Microgravity
18	Microgravity
19	Lunar
20	Lunar

Commercially-available starter motion capture systems. [1]recommended by company representative [2]not commercially available at time of writing

Company	System	Type	Price
Movella	Awinda Starter	Inertial	$4590
	MVN Link full body suit[1]	Inertial	$14,920
Qualisys	Miqus	Optical	$6000 per camera
	MiqusM3[1] (8 cameras)	Optical	$58,000 total
Vicon	Blue Trident	Inertial	$1600 per tracker
OptiTrack	Flex 3 (8-12 cameras)	Optical	$660 per camera
	PrimeX 13[1] (8-12 cameras)	Optical	$2500 per camera
	PrimeX 22[1] (8-12 cameras)	Optical	$4000 per camera
Noitom	Perception Neuron Studio[1]	Inertial	$7500
	Perception Neuron 3	Inertial	$4000
	Perception Neuron Pro[2]	Inertial	$2000

Specifications of the Raspberry Pi and Teensy 4.1 under trade study consideration. RedBoard is included for reference.

Specification	Raspberry Pi	Teensy 4.1	RedBoard
MicroSD slot	Yes	Yes	No
Power	3.3 V	3.3 V	3.3 V
Clock speed	**1-1.5 GHz**	600 MHz	16 MHz
I2C speed	400 kbit/sec	**1000 kbit/sec**	400 kbit/sec
# of I2C buses	2	**3**	1
Cost	**$25**	$29	$21
Footprint	36.4 cm^2	**10.8 cm^2**	36.5 cm^2

Microcontroller trade study criteria, weights, and results.

Criteria	Weight	Raspberry Pi	Teensy 4.1
Clock speed	1.5	1	0.5
I2C speed	1.5	0.4	1
# of I2C buses	3	0.6	1
Cost	1	1	0.9
Footprint	3	0.6	0.9
Total	10	6.7	**8.9**

Experimental setup for the adaptability statistical analysis. There is one independent variable with two factor levels and 10 trials each level for a total of $N = 20$.

Earth gravity	Microgravity
$N_1 = 10$	$N_2 = 10$

Experimental setup for the capability statistical analysis. There is one independent variable with three factor levels; there are 4, 4, and 2 trials per level for a total of $N = 10$.

1st parabolic section	2nd parabolic section	3rd parabolic section
$N_1 = 4$	$N_2 = 4$	$N_3 = 2$

Fluidity Indices for accelerometer/trial pairs. Each FI value is the time-averaged harmonic mean over each trial and accelerometer pair. Values are then averaged over all accelerometers for a 'whole body' FI mean and variance representing each trial. Mean values are used in comparison between ground and flight data, and variances are propagated forward for effect size calculations.

	Trial 1	Trial 2	$\cdots$	Trial 10
Accel 1	$FI_{1,1}$	$FI_{1,2}$	$\cdots$	$FI_{1,10}$
Accel 2	$FI_{2,1}$	$FI_{2,2}$	$\cdots$	$FI_{2,10}$
$\cdots$	$\cdots$	$\cdots$	$\cdots$	$\cdots$
Accel 12	$FI_{12,1}$	$FI_{12,2}$	$\cdots$	$FI_{12,10}$
$\downarrow$	$\downarrow$	$\downarrow$	$\downarrow$	$\downarrow$
Whole body	μ_1, σ_1^2	μ_2, σ_2^2	$\cdots$	μ_{10}, σ_{10}^2

Kruskal-Wallis one-way ANOVA results comparing fluidity values from parabolas in three different sections to understand longitudinal effects. The test was conducted at $\alpha = 0.05$ and * indicates significance.

Source	SS	df	MS	Chi-sq	Prob > Chi-sq
Groups	58	2	29	6.33	0.0423*
Error	24.5	7	3.5		
Total	82.5	9			

Summary of the pairwise comparison test for whole-body FI values from flight sections with the Bonferroni correction at an original significance of $\alpha = 0.05$, where * indicates significance. Mean rank statistics are from the Kruskal-Wallis test.

Section	Section	Mean rank difference	p-value
1	2	3	0.483
1	3	3.5	0.5458
1	3	6.5	0.0395*

Appendix B

Figures
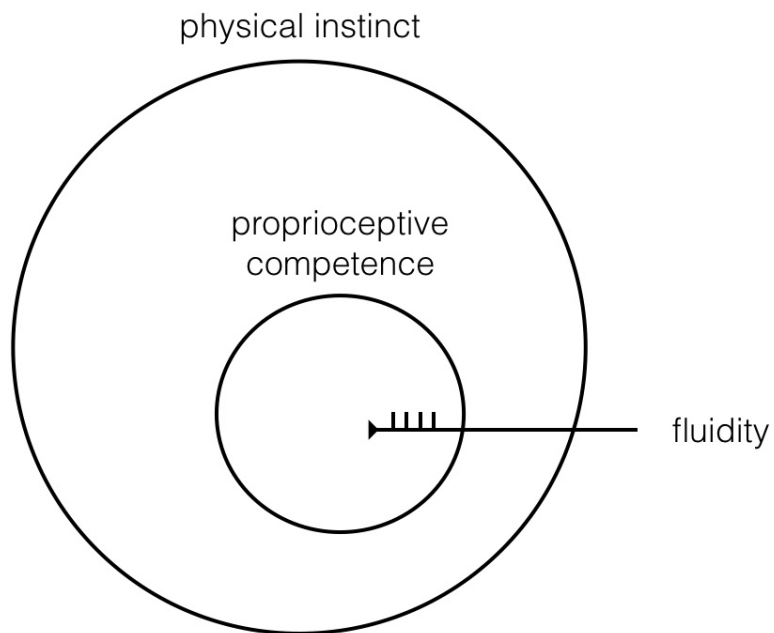
Proprioceptive competence, which we are coining here, is nested within all physical instinct (e.g. fluid shifts, cardiovascular changes, muscle atrophy in microgravity). Fluidity is proposed as a metric to measure proprioceptive competence, which has a two-part definition: adaptability to novel environments and capability of sustaining nominal tasks in the given environment.

Simplified block diagram of the first prototype. Four of these subsystems comprised the full whole-body system. Power and data streams are shown with solid and dashed arrows, respectively.
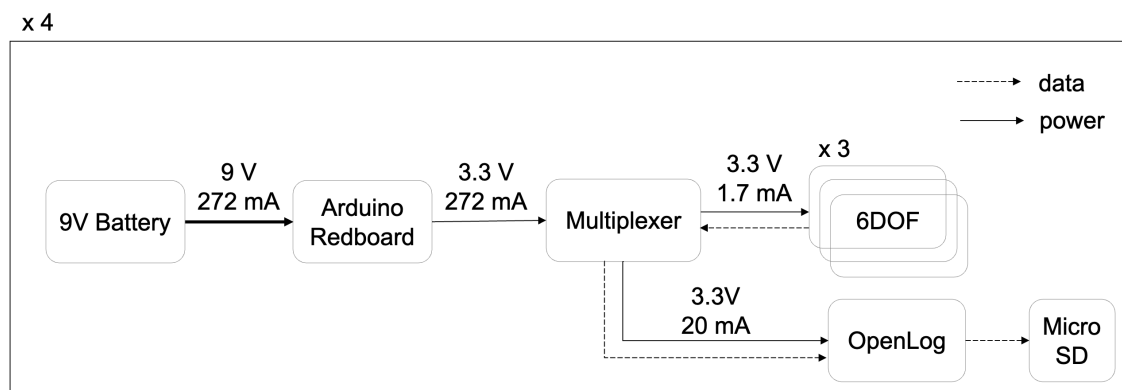
Simplified block diagram of the first prototype. Four of these subsystems comprised the full whole-body system. Power and data streams are shown with solid and dashed arrows, respectively.
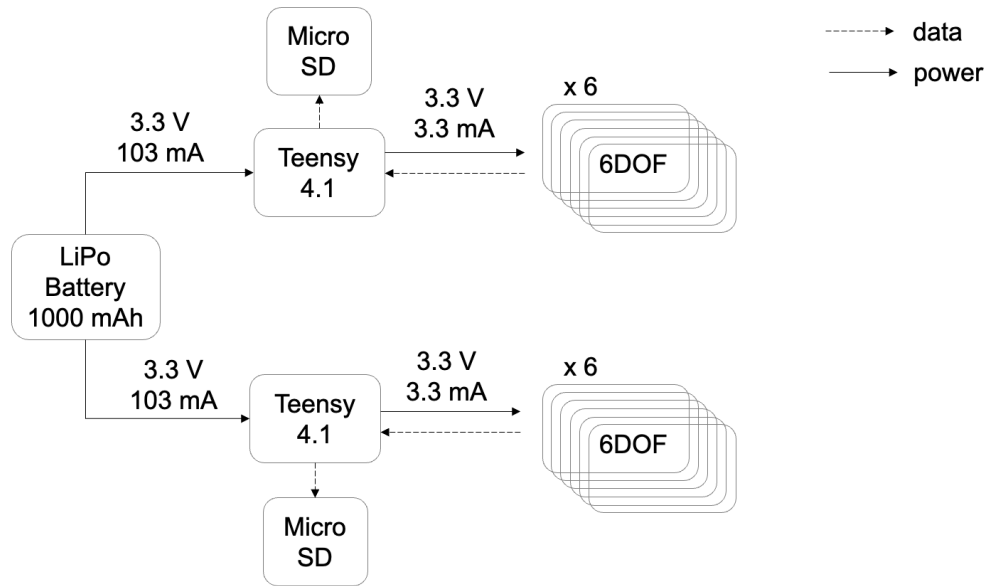
Simplified block diagram for the final prototype. Power and data streams are shown with solid and dashed arrows, respectively.

Full system wiring diagram of final flight-version system. Components are labeled from the top going counterclockwise. A (6DOF accelerometers); B (Teensy 4.1 microcontrollers); C (coin cell battery for RTC); D(battery backpack for LiPo recharging and supplying power); E (LiPo battery); F (microSD card).
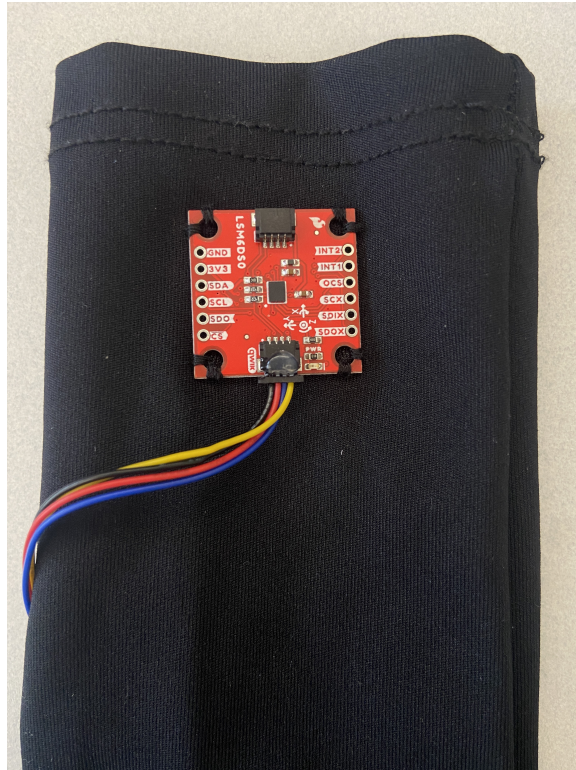
Hand-sewn detail of accelerometer attached to the garment at the wrist.

Final prototype garment close up.

Final prototype garment on-body.

Final prototype garment.
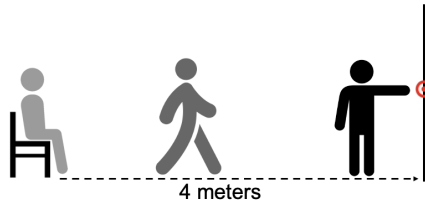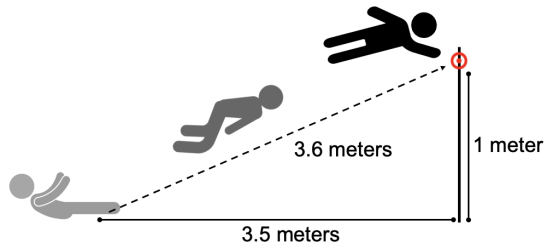
Ground experimental task   Flight experimental task

For the ground experiment, participants started in a seated position on a chair, then walked a distance of 4 meters, and touched the surface in front of them to conclude the traverse. For the flight experiment, participants started in a supine position on the plane floor, then traversed a distance of 3.6 meters, and touched the corner between the plane ceiling and the bulkhead wall to conclude the traverse.
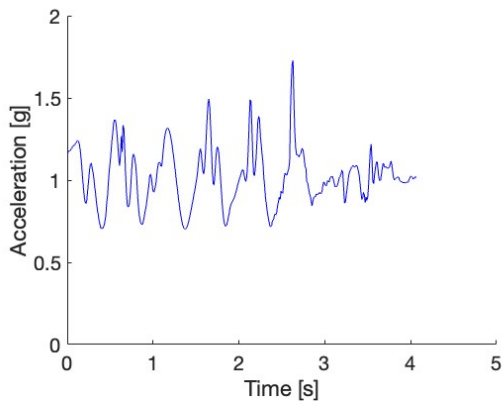
Ground acceleration data at original frequency of 100 Hz
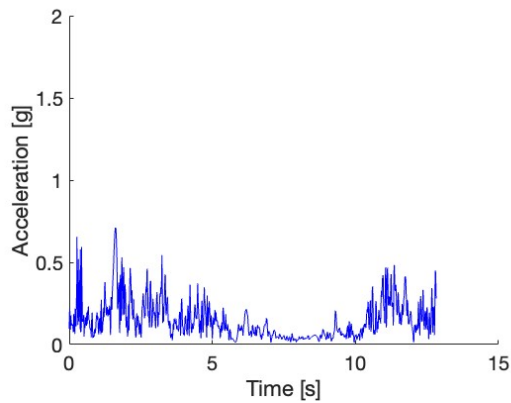
Flight acceleration data at original frequency of 100 Hz
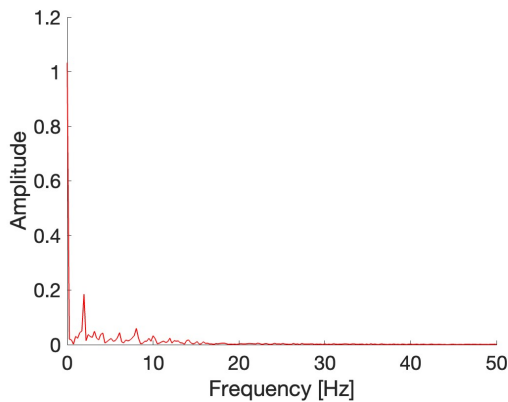
Ground FFT at original frequency of 100 Hz
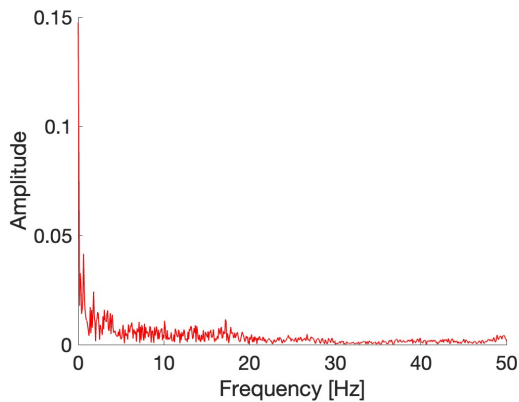
Flight FFT at original frequency of 100 Hz

Original frequency data for sample ground and flight acceleration from an example trial and accelerometer pair.
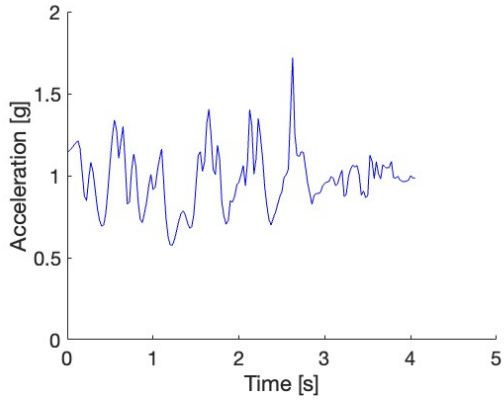
Ground acceleration at 40 Hz
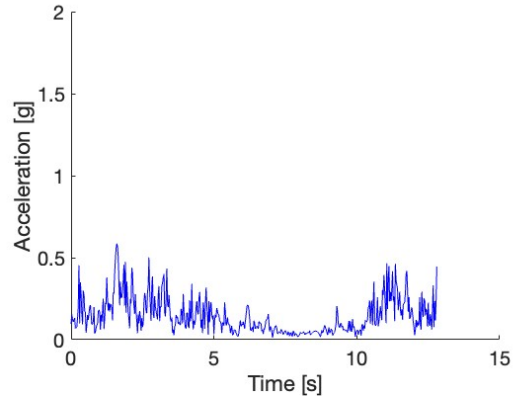
Flight acceleration data at 40 Hz
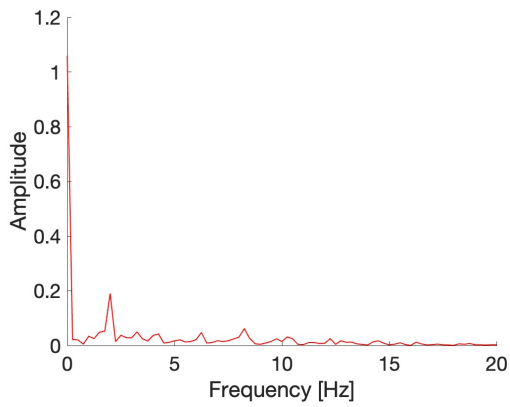
Ground FFT at 40 Hz
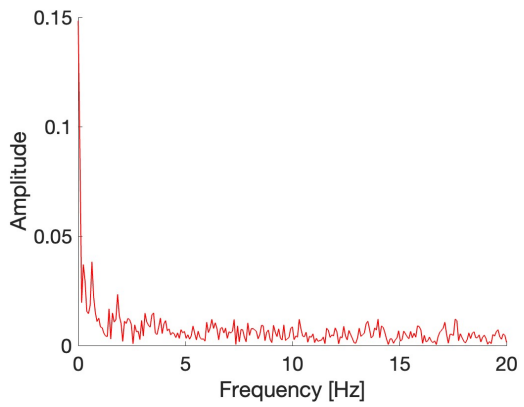
Flight FFT at 40 Hz

Downsampled (40 Hz) data for ground and flight acceleration from an example trial and accelerometer pair.
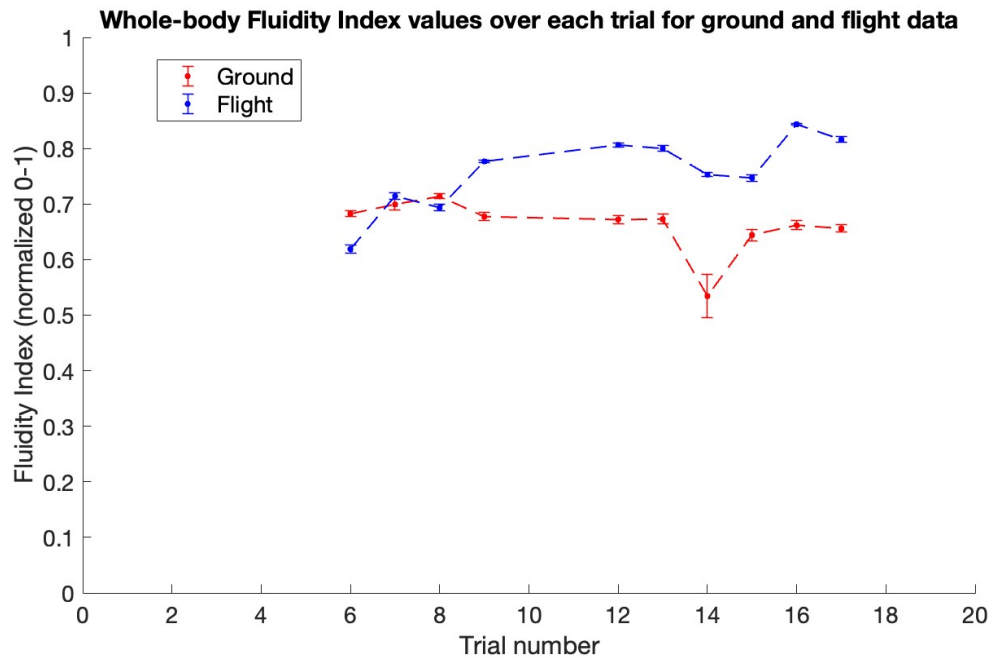
Whole-body Fluidity Index values (averaged over all accelerometers) for each trial are plotted for ground and flight conditions. Mean averaged joint FI values over each trial are plotted with variance error bars. Dashed lines are used for ground/flight grouping, but no data exists between the trials.
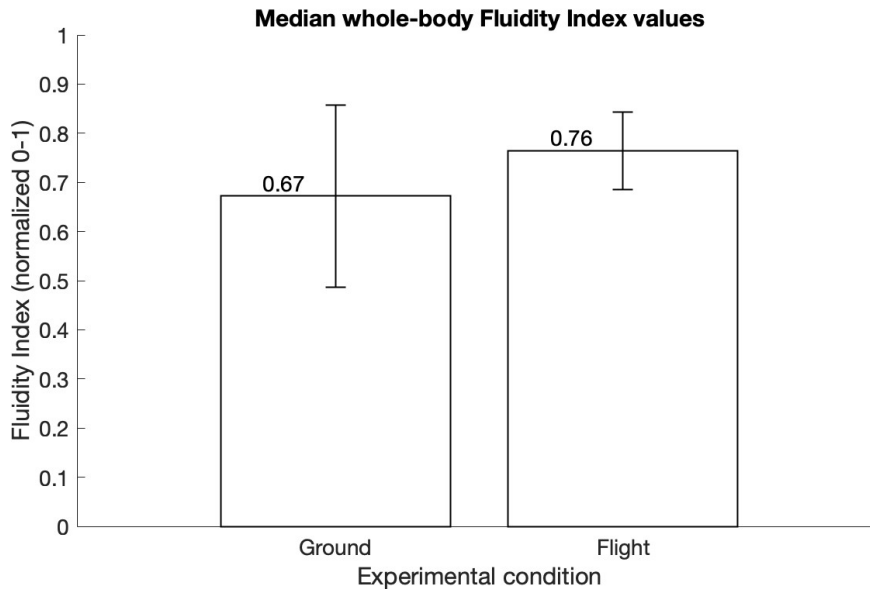
Median whole-body FI values over all trials for ground and flight conditions. Error bars are propagated variances from summed variances within run and covariances between trials.

Appendix C

COUHES Documentation

**CONSENT TO PARTICIPATE IN
BIOMEDICAL RESEARCH**

Physical Instinct in Microgravity

You have been asked to participate in a research study conducted by Michelle Lin from AeroAstro at the Massachusetts Institute of Technology (M.I.T.). The purpose of the study is to better understand the physical response to the microgravity environment. The results of this study may be included in Michelle Lin's Master's Thesis and PhD Dissertation. You were selected as a possible participant in this study because you participated in a microgravity flight provided by Zero Gravity Corporation in the May 2022 flight or another parabolic flight through the Space Exploration Initiative, or the 16.88 (or equivalent course number) course. You should read the information below, and ask questions about anything you do not understand, before deciding whether or not to participate.

The information below provides a summary of the research. Your participation in this research is voluntary and you can withdraw at any time.

- **Purpose**
  To better understand the physical response to the microgravity environment
- **Study Procedures**
  You will complete and repeat a translation task for data collection. You will wear a sensor-system garment, which will collect kinematic motion data.
- **Risks & Potential Discomfort**
  Discomfort may arise when the components on the garment press against the body. Please pause the experiment at any point to re-adjust the garment as needed. Risk of the microgravity flight itself may include discomfort and nausea.

You should read the information below, and ask questions about anything you do not understand before deciding whether or not to participate.

PARTICIPATION AND WITHDRAWAL

<u>EXPERIMENT</u>
Your participation in this research is completely VOLUNTARY. If you choose to participate you may subsequently withdraw from the study at any time without penalty or consequences of any kind. If you choose not to participate, that will not affect your relationship with M.I.T. or your right to health care or other services to which you are otherwise entitled.

<u>INTERVIEW</u>
• This interview is voluntary. You have the right not to answer any question, and to stop the interview at any time or for any reason. I expect that the interview will take about 30 minutes.

• This research will provide a better understanding to the physical responses that occur in a novel (microgravity) environment. There are no risks to this research.

• You will not be compensated for this interview.

• Unless you give us permission to use your name, title, and / or quote you in any publications that may result from this research, the information you tell us will be confidential.

• I would like to record this interview so that I can use it for reference while proceeding with this study. I will not record this interview without your permission. If you do grant permission for this conversation to be recorded, you have the right to revoke recording permission and/or end the interview at any time. Your withdrawl will not impact your grade in 16.88 (if applicable) or your relationship with Prof. Hoffman or Michelle Lin.

PURPOSE OF THE STUDY
The constant gravitation cue on Earth informs the neurovestibular and proprioceptive systems, which are systems in our bodies that control both how we interact with the external environment and how we move our bodies. Specifically, posture and limb movements rely on gravitational cues, and will behave differently in microgravity than on Earth. In an effort to understand the physical changes and short-term adaptation that occurs in microgravity, this experiment investigates physical instinct in microgravity. Specifically, a wearable sensor system in the form of a skintight garment (hereafter referred to as "garment") records angular acceleration and rotational motion data at each joint. The kinematic data from the joints will be used to assess joint jerk and be compared to a biomechanical model of the limbs to estimate the fluidity of movements. The data will provide insight into how fluidity changes in a novel gravity environment, and how that response changes over time.

PROCEDURES
GROUND EXPERIMENT
If you volunteer to participate in this study, we would ask you to do the following things prior to the day of flight on MIT campus:

We will measure your limb lengths and record your height and weight. You will be briefed on the system and understand how to operate the kill switch in case of emergency. You will be asked to put on the sensor system prior to the experiment. The garment goes under a flight suit, and we will power it on shortly before starting the experiment.

You will be asked to perform a translation task, which may involve sitting up from a chair, walking approximately 180 inches (about six steps), and touching a target. This will be repeated twenty (20) times. The length may vary, but will be no more than 100 feet (about 40 steps). If a translation is interrupted or otherwise incomplete, you may be asked to repeat that round again.

The entire experiment will be expected to take around an hour, including briefing and consenting. This study is voluntary and you may withdraw at any point.

FLIGHT EXPERIMENT
If you volunteer to participate in this study, we would ask you to do the following things on the day of flight at Pease, NH:

Pre-flight
This portion of the experiment is occurring for this study.

We will measure your limb lengths and record your height and weight. You will be briefed on the system and understand how to operate the kill switch in case of emergency. You will be asked to put on the sensor system prior to your microgravity flight. The garment goes under your flight suit, and we will power it on shortly before onboarding the flight.

<u>Flight</u>
This portion of the experiment is occurring for this study.
You will be asked to perform a translation task for each microgravity parabola of the flight. After nosing over, make your way to touch the opposite surface in the aircraft, then return to the aircraft floor to prepare for re-entry into hypergravity. No additional instructions on the mechanics of how to complete the task will be provided, please perform the task to the best of your interpretation.

<u>Post-flight</u>
This portion of the experiment is occurring for this study.
You will be asked to provide a detailed recounting of your flight experience, parabola by parabola. Please remember to note if you intentionally performed abnormal movements (e.g. somersault) during parabola(s). This interview is expected to take around 30 minutes and is voluntary.

<u>INTERVIEW</u>
As part of your participation, we will collect certain personal information about you, including: name, title, date(s) of flight, prior flight experience. We will ask you to complete a questionnaire and your answers will be recorded so we can analyze them after. You have the right to review your answers and withdraw your participation at any time.

Recordings and notes will be stored in a shared password-protected MIT Dropbox folder only accessible by key personnel. Each participant will be assigned a number code, with the form that associates the code to a specific person secured in a password-locked folder on MIT Dropbox. This folder will only be accessible by key personnel. The consent forms will also be stored in a separate password-protected MIT Dropbox folder, available to key personnel. All electronic data will be kept indefinitely.

This information will be retained indefinitely. You have the right to withdraw your data from the study at any time. To do so, contact Michell Lin [shuyulin@mit.edu]. If you withdraw from the study, no new information will be collected about you or from you by the study team. The data may be used for further research unrelated to the purpose of the current study, as a part of research efforts to comprehensively understand and analyze the human experience in microgravity environments.

POTENTIAL RISKS AND DISCOMFORTS

<u>Microgravity environment</u>
One risk of this study is short-term exposure to a microgravity environment. However, exposure to the microgravity environment is not a risk associated with this particular study, since the parabolic flight is taking place regardless of participation in this specific study, as you are chosen

from the registered flyers. A Medical History Form (attached), provided by the Zero-G Corporation, will be used to ensure that you are in good health or that a personal physician has determined that any existing medical condition(s) will not adversely affect the subject's participation in the ZERO-G flight. To further minimize the risks of microgravity, you will be trained on best practices in microgravity through the 18.66 course and/or the instruction of the Zero-G Corporation. Subjects will not be screened for motion sickness; however, the investigators will take several steps to ensure the comfort of the subjects. The investigators will recommend that you take an optional dose of anti-nausea medicine to counteract possible effects of nausea in microgravity. However, the investigator will not directly provide anti-nausea medication to you. Anti- nausea medicine will be completely optional, and you will only take the medication as approved by consultation with their personal doctor (either prescription scopolamine or over-the- counter Dramamine). During hypergravity periods you may rest in a static position, reducing the likelihood of nausea. If you need to take a break due to motion sickness, a portion of the aircraft is reserved as a "sick bay." In the case of medical emergency, the plane is immediately grounded and emergency medical personnel are called.

The risks associated with the flight itself are minimal. As with typical commercial flights, flight accidents are unlikely, but possible. Zero-G operates as a commercial flight operator under FAA regulations. The contract with Zero-G and all liability questions were formally reviewed by MIT RAS/OSP, who signed the contract on behalf of MIT.

Garment
The garment itself may also introduce discomfort, depending on the movements created. The battery has a risk of overheating, in which case you will need to trigger the kill switch.

The procedure may involve risks that are currently unforeseeable.

ANTICIPATED BENEFITS TO PARTICIPANTS
There are no anticipated benefits to you.

ANTICIPATED BENEFITS TO SOCIETY
The anticipated benefit of this study is a better understanding of joint kinematics and physical adaptation to novel gravity environments. The research will also be disseminated to the public in a lay manner, promoting accessibility for an otherwise very inaccessible experience.

ALTERNATIVES TO PARTICIPATION
The alternative is to not participate in the study.

PAYMENT FOR PARTICIPATION
You will not be paid for this study.

FINANCIAL OBLIGATION
Neither you nor your insurance company will be billed for your participation in this research.

PRIVACY AND CONFIDENTIALITY
The only people who will know that you are a research participant are members of the research team which might include outside collaborators not affiliated with MIT. No information about you, or provided by you during the research will be disclosed to others without your written permission, except: if necessary to protect your rights or welfare, or if required by law. In addition, your information may be reviewed by authorized MIT representatives to ensure compliance with MIT policies and procedures.

Video and audio recording may be used during the experiments. With your written permission, video/audio/visuals obtained from the experiment may be published or otherwise disseminated without further consent.

Once the experiment is completed, data/recordings/notes will be stored in a shared password-protected MIT Dropbox folder only accessible by key personnel. Each participant will be assigned a number code, with the form that associates the code to a specific person secured in a password-locked folder on MIT Dropbox. This folder will only be accessible by key personnel. The consent forms will also be stored in a separate password-protected MIT Dropbox folder, available to key personnel. All electronic data will be kept indefinitely.

WITHDRAWAL OF PARTICIPATION BY THE INVESTIGATOR
The investigator may withdraw you from participating in this research if circumstances arise which warrant doing so. If you experience any of the following side effects or if you become ill during the research, you may have to drop out, even if you would like to continue. The investigator, Michelle Lin, will make the decision and let you know if it is not possible for you to continue. The decision may be made either to protect your health and safety, or because it is part of the research plan that people who develop certain conditions may not continue to participate. Your withdrawl will not impact your grade in 16.88 (if applicable) or your relationship with Prof. Hoffman or Michelle Lin.

NEW FINDINGS
During the course of the study, you will be informed of any significant new findings (either good or bad), such as changes in the risks or benefits resulting from participation in the research or new alternatives to participation, that might cause you to change your mind about continuing in the study. If new information is provided to you, your consent to continue participating in this study will be re-obtained.

EMERGENCY CARE AND COMPENSATION FOR INJURY

If you feel you have suffered an injury, which may include emotional trauma, as a result of participating in this study, please contact the person in charge of the study as soon as possible.

In the event you suffer such an injury, M.I.T. may provide itself, or arrange for the provision of, emergency transport or medical treatment, including emergency treatment and follow-up care, as needed, or reimbursement for such medical services. M.I.T. does not provide any other form of compensation for injury. In any case, neither the offer to provide medical assistance, nor the actual provision of medical services shall be considered an admission of fault or acceptance of liability. Questions regarding this policy may be directed to MIT's Insurance Office, (617) 253-2823.

IDENTIFICATION OF INVESTIGATORS

In the event of a research related injury or if you experience an adverse reaction, please immediately contact one of the investigators listed below. If you have any questions about the research, please feel free to contact:
Jeffrey Hoffman, Principle Investigator, 70 Vassar St., Cambridge, MA
Michelle Lin, Co-Investigator, (720) 756-6985, 41 Vassar St., Cambridge, MA

RIGHTS OF RESEARCH SUBJECTS

You are not waiving any legal claims, rights or remedies because of your participation in this research study. If you feel you have been treated unfairly, or you have questions regarding your rights as a research subject, you may contact the Chairman of the Committee on the Use of Humans as Experimental Subjects, M.I.T., Room E25-143B, 77 Massachusetts Ave, Cambridge, MA 02139, phone 1-617-253 6787.

As part of your participation, we will collect certain personal information about you, including: name, title, date(s) of flight, prior flight experience.

The purpose of the data collection is to gather anecdotes regarding the physical instincts and responses experienced during a microgravity flight, in particular during the first exposure to microgravity. The information you provide will only be available to MIT. Your data will be secured through the following methods: the recordings will be transferred to an encrypted hard drive within 24 hours after the recording is complete, the original recording will be deleted permanently, and the hard drive will be under double-lock on MIT campus.

This information will be retained indefinitely. You have the right to withdraw your data from the study at any time. To do so, contact Michell Lin [shuyulin@mit.edu]. If you withdraw from the study, no new information will be collected about you or from you by the study team. The data may be used for further research unrelated to the purpose of the current study, as a part of research efforts to comprehensively understand and analyze the human experience in microgravity environments.

If you are a student or lab member of Jeffrey Hoffman, your decision to participate or not to participate will not in anyway influence your grade, funding, or other relationship with Jeffrey Hoffman.

SIGNATURE OF RESEARCH SUBJECT OR LEGAL REPRESENTATIVE

I have read (or someone has read to me) the information provided above. I understand the procedures described above. I have been given an opportunity to ask questions and all of my questions have been answered to my satisfaction. I have been given a copy of this form.

(*Please check all that apply*)

[ ] I give permission for this interview to be recorded.

[ ] I give permission for the following information to be included in publications resulting from this study:

[ ] my name   [ ] my title   [ ] direct quotes from this interview

BY SIGNING THIS FORM, I WILLINGLY AGREE TO PARTICIPATE IN THE RESEARCH IT DESCRIBES.

_____
Name of Subject

_____
Name of Legal Representative (if applicable)

_____   _____
Signature of Subject or Legal Representative   Date

SIGNATURE OF PERSON OBTAINING INFORMED CONSENT

I have explained the research to the participant or his/her legal representative, and answered all of his/her questions. I believe that he/she understands the information described in this document and freely consents to participate.

_____
Name of Person Obtaining Informed Consent

_____   _____
Signature of Person Obtaining Informed Consent   Date (must be the same as subject's)

Please contact Michelle Lin [shuyulin@mit.edu] any questions or concerns.

If you feel you have been treated unfairly, or you have questions regarding your rights as a research subject, you may contact the Chairman of the Committee on the Use of Humans as Experimental Subjects, M.I.T., Room E25-143b, 77 Massachusetts Ave, Cambridge, MA 02139, phone 1-617-253-6787.

Appendix D

Code

Data cleaning

```
1  %% FilesToStruct
2  %
3  % Purpose: Takes two data files of identical dimentions.
      Time is converted
4  % to milliseconds and zeroed based on whichever file has
      the earlier
5  % initial time value. Renames the IMUs of the second file
      to be 7-12 rather
6  % than 1-6. Splits data at "Data Collection" headers, and
      combines
7  % horizontally across both data files by stacking them
      vertically (file 1
8  % on top of file 2) and adding it to a field of a
      Structure. Result in
9  % SRuns. It then splits runs into fields of same IMU
      numbers. Result in
10 % SRunsIMUs.
11 %
12 % For example,
13 % data group between header 1 and 2 in File 1 goes on top
      of data group
14 % between header 1 and 2 in File 2. These two groups are
      stored in the same
15 % field named Run_1. Same goes for between header 2 and 3
      in Run_2. Within
```

```matlab
16 % these fields, data is placed into new fields by IMU # (
     ex. Run_1_IMU_4)
17 % Meant to work for all data files.
18 %
19 % Author: Caitlin Lian (calian@mit.edu)
20 % Date Created: Oct 18, 2022
21 % Date Last Modified: Dec 5, 2022
22
23
24
25 %% House keeping
26 clear; clc; close all;
27
28 %% Fetch File
29 % filename1 = 'flight_data_1.txt';
30 % filename2 = 'flight_data_2.txt';
31 filename1 = 'ground_test_1.txt';
32 filename2 = 'ground_test_2.txt';
33
34 %% Import Options
35 %dateTimeFormat = 'hh:mm:ss SSS';
36 %varNames = {'Time', 'IMU', 'X_Pos', 'Y_Pos', 'Z_Pos', '
     X_Gyro', 'Y_Gyro', 'Z_Gyro'};
37 delimiter = ',';
38 extraColRule = 'ignore';
39 dataStartLine = 1;
40
41 opts = delimitedTextImportOptions('Delimiter',delimiter,...
42                                   'DataLines', dataStartLine
                                      );
43
44 %% Read Matrix Here
45 Data1 = readmatrix(filename1, opts);
46 Data2 = readmatrix(filename2, opts);
47
48 %% Allocate Columns to Vars
49 time1 = Data1(:,1);
50 time2 = Data2(:,1);
51 imu1 = str2double(Data1(:,2));
52 imu2 = str2double(Data2(:,2));
53 x_pos1 = str2double(Data1(:,3))/10000;
54 x_pos2 = str2double(Data2(:,3))/10000;
55 y_pos1 = str2double(Data1(:,4))/10000;
56 y_pos2 = str2double(Data2(:,4))/10000;
57 z_pos1 = str2double(Data1(:,5))/10000;
```

```matlab
58  z_pos2 = str2double(Data2(:,5))/10000;
59  x_gyro1 = str2double(Data1(:,6))/10000;
60  x_gyro2 = str2double(Data2(:,6))/10000;
61  y_gyro1 = str2double(Data1(:,7))/10000;
62  y_gyro2 = str2double(Data2(:,7))/10000;
63  z_gyro1 = str2double(Data1(:,8))/10000;
64  z_gyro2 = str2double(Data2(:,8))/10000;
65
66  %% Time Conversion Operations
67  %%Convert to datetime:
68  time1 = datetime(time1,'InputFormat','HH:mm:ss SSS');
69  time2 = datetime(time2,'InputFormat','HH:mm:ss SSS');
70
71  %%Uncallibrated:
72  time1 = convertToMS(hour(time1), minute(time1), second(
        time1))/1000; %Stays in seconds
73  time2 = convertToMS(hour(time2), minute(time2), second(
        time2))/1000;
74
75  %%Zero based on which started first
76  if time1(2) < time2(2)
77      time2 = time2 - time1(2);
78      time1 = time1 - time1(2);
79  else
80      time1 = time1 - time2(2);
81      time2 = time2 - time2(2);
82  end
83
84  %% Change IMUs of data 2
85  % We use search and replace rather than finding every 6th
        element to avoid
86  % header conflicts
87  imu2(imu2==1) = 7;
88  imu2(imu2==2) = 8;
89  imu2(imu2==3) = 9;
90  imu2(imu2==4) = 10;
91  imu2(imu2==5) = 11;
92  imu2(imu2==6) = 12;
93
94  %% Combine into two matrices
95  AllRuns1 = cat(2, time1, imu1, x_pos1, y_pos1, z_pos1,
        x_gyro1, y_gyro1, z_gyro1);
96  AllRuns2 = cat(2, time2, imu2, x_pos2, y_pos2, z_pos2,
        x_gyro2, z_gyro2, y_gyro2);
97
```

```matlab
 98  %% Splitting data by run and recombining correctly
 99  % Uses indexes of headers to split into matrices. Stacks
         this
100  % from data file 1 and data file 2 vertically. Repeats
         when next header is
101  % found. At the end, it creates one last field containing
         matrix rows from
102  % last header to the end from data file 1 and 2 stacked
         vertically. Needs a
103  % header for it to work or else struct will be empty!
104
105  allHeaderIndexes1 = find(isnan(AllRuns1(:,1))); %Find
         index of each header
106  allHeaderIndexes2 = find(isnan(AllRuns2(:,1))); %Find
         index of each header
107
108  if size(allHeaderIndexes1) ~= size(allHeaderIndexes2)
109      disp 'Doesn't have same number of headers. Cannot
             struct
110  else
111      newMatrixCount = 0;
112      SRuns = struct;
113
114          for i = 1:size(allHeaderIndexes1 ,1)
115          newMatrixCount = newMatrixCount + 1;
116          name = strcat('Run_', num2str(newMatrixCount));
117          % Assigns matrix from file 1 and 2 to G1 and G2
                 respectively
118          % from one after current header to one before next
                 header of each
119          % file
120          beginIndex1 = allHeaderIndexes1(i)+1;
121          beginIndex2 = allHeaderIndexes2(i)+1;
122              if i~=size(allHeaderIndexes1 ,1)
123                  endIndex1 = allHeaderIndexes1(i+1)-1;
124                  endIndex2 = allHeaderIndexes2(i+1)-1;
125                  G1 = AllRuns1(beginIndex1: endIndex1, :);
126                  G2 = AllRuns2(beginIndex2: endIndex2, :);
127              else % the end case
128                  G1 = AllRuns1(beginIndex1: end, :);
129                  G2 = AllRuns2(beginIndex2: end, :);
130              end
131
132          %Create the field
133          [SRuns(:).(name)] = vertcat(G1,G2);
```

```matlab
134              clear G1 G2;
135          end
136 end
137
138 %% Splitting fields by IMU , creating new fields in new
        struct
139 % For each run in S, look for each imu = j, add to
        Run_1_IMUj
140 % Note: this could be made more efficient if the two files
         are not
141 % combined , and we search for 1-6 from file 1 and 7-12
        from file 2. It was
142 % not done this way because we may need access to the runs
         not split by
143 % IMUs .
144
145 SRunsIMUs = struct ;
146 sfieldnames = fieldnames ( SRuns );
147 for i = 1: length ( sfieldnames )
148     f = SRuns .( char ( sfieldnames (i)));
149     for j = 1:12
150         name = strcat ( char ( sfieldnames (i)),'_IMU_',
                num2str (j));
151         imumatrix = f(f(:,2)==j, :);
152         [SRunsIMUs (:).( name )] = imumatrix ;
153     end
154 end
155
156
157 %% FUNCTIONS %%
158 % Convert to milliseconds , param hours , minutes , seconds
159 function totalMS = convertToMS (h, m, s)
160     %% Time Conversion Values
161     msph = 3600000;
162     mspm = 60000;
163     msps = 1000;
164     totalMS = h* msph + m* mspm + s* msps ;
165 end
```

Downsampling

```matlab
1 %% plotting acceleration data
2 % plotting accel data by runs , downsampling visualization
      of accel
3 % low pass filter and downsampling processes
```

```matlab
4  %
5  % Author: Michelle Lin
6  % Date created: Mar 15, 2023
7  % Date last modified: May 7, 2023
8
9  %% Housekeeping
10 clc; clear all; close all;
11
12 %% set global variables
13 global Fs
14 Fs = 40; % [hz] set downsampling frequency
15
16 %% get accel (& downsampled accel) structs
17 % interested runs 5, 6, 7, 8, 11-16
18 runs = [5, 6, 7, 8, 11:16];
19 % runs = [1:16];
20 % get ground and flight original and downsampled
       accelerations
21 [ground_accel_data] = process_accel_data('ground',runs);
22 [flight_accel_data] = process_accel_data('flight',runs);
23
24 %% plot accel and jerk for ground and flight
25 % ground
26 % assign variables
27 ground_accel(:,1) = ground_accel_data.Run_13.IMU_1.time_d;
28 ground_accel(:,2) = ground_accel_data.Run_13.IMU_1.accel_d
       ;
29 ground_jerk(:,1) = ground_accel(2:end,1); % [s] time (
       shifted for diff)
30 ground_jerk(:,2) = diff(ground_accel(:,2))./diff(
       ground_accel(:,1));
31
32 figure
33 axes('FontSize', 20, 'NextPlot', 'add');
34 hold on
35 plot(ground_accel(:,1), ground_accel(:,2), 'b','LineWidth'
       ,1)
36 xlabel('Time [s]');ylabel('Acceleration [g]')
37 ylim([0 2])
38
39 % flight
40 flight_accel(:,1) = flight_accel_data.Run_13.IMU_1.time_d;
41 flight_accel(:,2) = flight_accel_data.Run_13.IMU_1.accel_d
       ;
42 flight_jerk(:,1) = flight_accel(2:end,1); % [s] time (
```

```matlab
      shifted for diff)
43 flight_jerk(:,2) = diff(flight_accel(:,2))./diff(
      flight_accel(:,1));
44
45 figure
46 axes('FontSize', 20, 'NextPlot', 'add');
47 hold on
48 plot(flight_accel(:,1), flight_accel(:,2), 'b','LineWidth'
      ,1)
49 xlabel('Time [s]');ylabel('Acceleration [g]')
50 ylim([0 2])
51
52
53 % % check frequency profiles
54 L = 500; % change to even length of vector
55 t = flight_accel(:,1); % change
56 S = flight_accel(:,2); % change
57 Y = fft(S);
58 P2 = abs(Y/L);
59 P1 = P2(1:L/2+1);
60 P1(2:end-1) = 2*P1(2:end-1);
61 f = Fs*(0:(L/2))/L;
62
63 figure
64 axes('FontSize', 20, 'NextPlot', 'add');
65 hold on
66 plot(f,P1,'r','LineWidth',1)
67 xlabel('Frequency [Hz]');ylabel('Amplitude')
68 abel('jerk [g/s]')
69 %
70 %
71 % figure
72 % hold on
73 % subplot(2,1,1)
74 % hold on
75 % plot(flight_orig_accel(:,1), flight_orig_accel(:,2),'b
      ','LineWidth',1)
76 % plot(flight_downsample_accel(:,1),
      flight_downsample_accel(:,2),'*r')
77 % legend('original data [100 hz]', sprintf('downsampled
      data [%d hz]',new_rate))
78 % title('Flight accel data (run 5 imu 1) vs downsampled
      data');xlabel('time [s]');ylabel('accel [g]')
79 % % plotting jerk
80 % subplot(2,1,2)
```

```
81  % hold on
82  % plot(flight_orig_jerk(:,1), flight_orig_jerk(:,2), 'b','
       LineWidth',1)
83  % plot(flight_downsample_jerk(:,1), flight_downsample_jerk
       (:,2), '*r')
84  % legend('original data [100 hz]',sprintf('downsampled
       data [%d hz]',new_rate))
85  % title('Ground jerk data (run 5 imu 1) vs downsampled
       data');xlabel('time [s]');ylabel('jerk [g/s]')
86
87  %% low pass filter and downsampling
88  % % check of frequency content for flight data (pretty
       consistent decline
89  % % through 50 hz, no particular machine freq standing out
       )
90  %
91  % Fs = 100; % [hz] freqency is 100 hz
92  % T = 1/Fs; % [s] period is 0.01 seconds
93  % L = 1380; % set length to be smaller for interp, even
94  % t = (0:L-1)*T; % time vector
95  %
96  % S = interp1(flight_orig_accel(:,1)-flight_orig_accel
       (1,1),flight_orig_accel(:,2),t); % interpolate to fft
       time vec
97  % % time has to start from 0 so subtract the first index
98  %
99  % % check interp fit
100 % figure
101 % plot(t, S)
102 % hold on
103 % plot(flight_orig_accel(:,1)-flight_orig_accel(1,1),
       flight_orig_accel(:,2),'r')
104 %
105 % Y = fft(S); % take fft
106 %
107 % P2 = abs(Y/L);
108 % P1 = P2(1:L/2+1);
109 % P1(2:end-1) = 2*P1(2:end-1);
110 %
111 % f = Fs*(0:(L/2))/L;
112 %
113 % plot(f,P1)
114 %
115 % % ground check (freq mostly below 15 hz)
116 % % check of frequency content
```

```
117 % Fs = 100; % [hz] freqency is 100 hz
118 % T = 1/Fs; % [s] period is 0.01 seconds
119 % L = 584; % set length to be smaller for interp, even
120 % t = (0:L-1)*T; % time vector
121 %
122 % S = interp1(ground_orig_accel(:,1)-ground_orig_accel
       (1,1),ground_orig_accel(:,2),t); % interpolate to fft
       time vec
123 % % time has to start from 0 so subtract the first index
124 %
125 % Y = fft(S); % take fft
126 %
127 % P2 = abs(Y/L);
128 % P1 = P2(1:L/2+1);
129 % P1(2:end-1) = 2*P1(2:end-1);
130 %
131 % f = Fs*(0:(L/2))/L;
132 %
133 % plot(f,P1)
```

Data analysis code

```
 1 %% Data Analysis
 2 % Analyzing fluidity data from ground and flight, saving
       to variables to
 3 % plot mean_ground vs mean_flight, testing for normality
       and
 4 % homoscedasticity, effect size and power analysis calcs
 5
 6 % Author: Michelle Lin (shuyulin)
 7 % Date created: 6 Mar 2023
 8 % Date last modified: 24 Mar 2023
 9
10 %% Housekeeping
11 clc; close all; clear all;
12
13 %% calculate jerk and fluidity
14 % interested runs 1 through 16
15 % 1- RS
16 % 2- LS
17 % 3 - LE
18 % 4- LH
19 % 5- LK
20 % 6- LA
21 % 7- RHip
```

```matlab
% 8- Lhip
% 9 - RK
% 10 -RA
% 11- RE
% 12- RH
imu_num = [1:12];
% imu_num= [5:10]; % lower body
% imu_num = [1:4 11:12]; % upper body
% imu_num = [1:3 5 7:9 11]; %core body
% imu_num = [4 6 10 12]; % extremities
run_num = [5, 6, 7, 8, 11:16];
% runs in terms of the whole flight
run_names = [6, 7, 8, 9, 12, 13, 14, 15, 16,17];

ground_struct = fluiditycalc('ground',run_num);
flight_struct = fluiditycalc('flight',run_num);

[ground_datasummary, cov_g] = statprocess(run_num, imu_num
    , ground_struct);
[flight_datasummary, cov_f] = statprocess(run_num, imu_num
    , flight_struct);

%% descriptive statistics for ground vs flight data,
    flight data
% plotting ground summary w/ variance as error
figure
axes('FontSize', 14, 'NextPlot', 'add');
hold on
errorbar(run_names, ground_datasummary(1,:),
    ground_datasummary(2,:),'r.','LineWidth',0.8,'
    MarkerSize',10)
plot(run_names, ground_datasummary(1,:),'r--','LineWidth'
    ,1)
errorbar(run_names, flight_datasummary(1,:),
    flight_datasummary(2,:),'b.','LineWidth',0.8,'
    MarkerSize',10)
plot(run_names, flight_datasummary(1,:),'b--','LineWidth'
    ,1)
xlim([0 20]);ylim([0 1])
legend({'Ground','','Flight',''},'FontSize',14)
xlabel('Trial number');ylabel('Fluidity Index (normalized
    0-1)')
title('Whole-body Fluidity Index values over each trial
    for ground and flight data','FontSize',15)
```

```matlab
56
57  %% effect size and power analysis
58  % use cohen's d (mu1-mu2)/s, s = sqrt(s1^2 + s2^2 /2)
59  mu1 = mean(ground_datasummary(1,:));
60  mu2 = mean(flight_datasummary(1,:));
61
62  s1 = sum(ground_datasummary(2,:))+trace(flip(cov_g));
63  s2 = sum(flight_datasummary(2,:))+trace(flip(cov_f));
64
65  d = abs(mu1-mu2)/sqrt((s1^2 + s2^2)/2);
66
67  % use hedge's g for small sample correction, df = n1+n2-2
       = 18
68  df = 10+10-2;
69
70  g = d*(1 - 3/(4*df - 1));
71
72  % projected effect size
73  effsize = 0.3;
74  n = 20;
75  alpha = 0.05;
76  zalph = 2.101; %using t table df= 18
77
78  % n = ((zalph + zbeta)/effsize)^2
79
80  zbeta = sqrt(n)*effsize - zalph;
81
82  beta = 1- 0.267;
83  %% test for equal variances across ground and flight data
84  % normality test for ground runs and flight runs (2 vecs)
85  % h = 0 means data comes from a normal distribution, h=1
       means reject null
86  [h_gn, p_gn] = kstest(ground_datasummary(1,:))
87
88  fprintf('ground runs has h = %d \n',h_gn)
89
90  [h_fn,p_fn] = kstest(flight_datasummary(1,:))
91
92  fprintf('ground runs has h = %d \n',h_fn)
93  % variance testing using levene's test (bartlett's test
       has sensitivity to
94  % nonnormality)
95  % do the ground and flight data (as col vec) have the same
        variance?
96  % h=0 means equal variance; h=1 means unequal
```

```matlab
 97  [p_v, stats_v] =vartestn([ground_datasummary(1,:)',
        flight_datasummary(1,:)'],'TestType','LeveneAbsolute')
 98
 99  % p = 0.025, rejects null, suggesting we cannot assume
        equal variances
100  %% adaptability testing
101  % wilcoxon two-tailed signed rank test for dependent
        samples
102  % h0 = they are from the same distributions
103  % ha = they are from different distributions
104  [p_a,h_a,stats_a] = signrank(ground_datasummary(1,:),
        flight_datasummary(1,:));
105  % p = 0.0137; h=1, which means we can reject the null
        hypothesis at 5%
106  % significance
107
108  x_bar = categorical({'Ground', 'Flight'});
109  x_bar = reordercats(x_bar, {'Ground','Flight'});
110  y_bar = [median(ground_datasummary(1,:)) median(
        flight_datasummary(1,:))];
111
112
113  figure
114  hold on
115  set(gca, 'FontSize',14)
116  b = bar(x_bar,y_bar,'w','LineWidth',1);
117  errorbar(x_bar,y_bar,[s1 s2],'k','LineStyle','none','
        LineWidth',1,'CapSize',12)
118  text(x_bar(1),y_bar(1),'0.67      ','VerticalAlignment','
        bottom','HorizontalAlignment','right','FontSize',14)
119  text(x_bar(2),y_bar(2),'0.76      ','VerticalAlignment','
        bottom','HorizontalAlignment','right','FontSize',14)
120
121  ylim([0 1])
122  xlabel('Experimental condition');ylabel('Fluidity Index (
        normalized 0-1)')
123  title('Median whole-body Fluidity Index values','FontSize'
        ,15)
124
125
126  %% capability testing
127  groups = {'1','1','1','1','2','2','2','2','3','3'};
128
129  figure
130  [p_f, tbl, stats] = kruskalwallis(flight_datasummary(1,:),
```

```
        groups );
131
132 figure
133 c = multcompare ( stats ,"CriticalValueType","bonferroni");
134 %% legacy code
135 % % load data
136 % ground_struct = load ('ground_fluiditydata.mat');
137 % flight_struct = load ('flight_fluiditydata.mat');
138
139 % % ground data processing
140 % % interested IMUs 1 through 12
141 % imu_num = [1:12];
142 %
143 % % make matrix to hold means and variances
144 % % where the first sheet is the means and the second
      sheet is the variances
145 % ground_datasummary = zeros (length (run_num), length (
      imu_num), 3);
146 % % empty vectors for variance testing
147 % ground_data = [];
148 % ground_category = [];
149 %
150 % % for loop to run through the interested runs
151 % for i = 1: length (run_num)
152 % %      another for loop for IMUs
153 %     for j = 1: length (imu_num)
154 % %          current working vector, col1 = time, col2 =
      fluidity values
155 %          data = getfield (ground_struct.SFluidity, sprintf
      ('Ground_Run_%d_IMU_%d', i, j));
156 % %          set mean into appropriate space on sheet 1
157 %          ground_datasummary (i, j, 1) = mean (data (:,2));
158 % %          set variance into appropriate space on sheet 2
159 %          ground_datasummary (i, j, 2) = var (data (:,2));
160 % %          set standard deviation into appropriate space
      on sheet 3
161 %          ground_datasummary (i, j, 3) = std (data (:,2));
162 %
163 % %          test for normality with shifted mean and std
164 %          if kstest ((data (:,2)-mean (data (:,2)))/std (data
      (:,2)))==0
165 %              fprintf ('data is normal')
166 %          end
167 %
168 % %          append data to make big vector for variance
```

```
        test
169 %           ground_data = [ground_data; data(:,2)];
170 % %          make categories for Bartlett variance test '#
        run#imu'
171 %           ground_category = [ground_category; str2num(
        sprintf('%d%d',i,j))*ones(length(data(:,2)),1)];
172 %
173 %     end
174 % end
175 %
176 % % flight data processing
177 % % interested runs 5, 6, 7, 8, 11-16
178 % run_num = [5 6 7 8 11:16];
179 % % interested IMUs 1 through 12
180 % imu_num = [1:12];
181 %
182 % % make matrix to hold means and variances
183 % % where the first sheet is the means and the second
        sheet is the variances
184 % flight_datasummary = zeros(length(run_num), length(
        imu_num), 2);
185 % % empty vectors for variance testing
186 % flight_data = [];
187 % flight_category = [];
188 %
189 % % for loop to run through the interested runs
190 % for i = 1:length(run_num)
191 % %     another for loop for IMUs
192 %     for j = 1:length(imu_num)
193 % %         current working vector, col1 = time, col2 =
        fluidity values
194 %         data = getfield(flight_struct.SFluidity,sprintf
        ('Flight_Run_%d_IMU_%d',run_num(i),j));
195 % %         set mean into appropriate space on sheet 1
196 %         flight_datasummary(i, j, 1) = mean(data(:,2));
197 % %         set variance into appropriate space on sheet 2
198 %         flight_datasummary(i, j, 2) = var(data(:,2));
199 % %         set standard deviation into appropriate space
        on sheet 3
200 %         flight_datasummary(i, j, 3) = std(data(:,2));
201 % %         test for normality with shifted mean and std
202 %         if kstest((data(:,2)-mean(data(:,2)))/std(data
        (:,2)))==0
203 %             fprintf('data is normal')
204 %         end
```

```
205 %
206 % %             append data to make big vector for variance
        test
207 %             flight_data = [flight_data; data(:,2)];
208 % %           make categories for Bartlett variance test '#
        run#imu'
209 %             flight_category = [flight_category; str2num(
        sprintf('%d%d',i,j))*ones(length(data(:,2)),1)];
210 %        end
211 % end
212
213 % % plotting ground summary w/ variance as error
214 %
215 % figure
216 % sgtitle('Average fluidity values over each run for
        ground and flight data')
217 % hold on
218 % % make 12 subplots for 12 imus
219 % for i = 1:12
220 %      subplot(3,4,i)
221 %      for j = 1:10
222 %           hold on
223 %           errorbar(1,ground_datasummary(j, i, 1),
        ground_datasummary(j, i, 2),'r.')
224 %           ylim([0 1]); xlim([0 3]);
225 %           ylabel('Fluidity');
226 %      end
227 %      for j = 1:10
228 %           hold on
229 %           errorbar(2,flight_datasummary(j, i, 1),
        flight_datasummary(j, i, 2),'bo')
230 %      end
231 % end
232 %
233 % figure
234 % hold on
235 % sgtitle('Average fluidity values over each flight
        parabola')
236 % % make 12 subplots for 12 imus
237 % for i = 1:12
238 %      subplot(3,4,i)
239 %      for j = 1:10
240 %           hold on
241 %           errorbar(j,flight_datasummary(j, i, 1),
        flight_datasummary(j, i, 2),'bo')
```

```
242 %           xlabel('Parabola'); ylabel('Fluidity')
243 %           xlim([0 13]); ylim([0 1]);
244 %           vfill([4.5 8.5], 'gray','facealpha',.05);
245 %       end
246 % end
```

Data processing

```
 1 % author: michelle lin (shuyulin)
 2 % accel data into struct by runs and imus (sqrt of squared
      sums across xyz components)
 3 % downsampling to global Fs hz
 4 % can choose between a spline interp, resample, spline
      resample, or lowpass
 5 % w/ spline interp options.
 6
 7 % date created: mar 25 2023
 8 % date last modified: mar 25 2023
 9
10 function endStruct = process_accel_data(trial, runs)
11 global Fs
12
13     if trial == 'flight'
14         load('Flight_Data_By_Run_IMU', 'SRunsIMUs')
15     elseif trial == 'ground'
16         load('Ground_Test_By_Run_IMU', 'SRunsIMUs')
17     else
18         fprintf('need to enter flight or ground as string'
            )
19     end
20
21 % make new structs
22 endStruct.Run_1 = [];
23 endStruct.Run_2 = [];
24 endStruct.Run_3 = [];
25 endStruct.Run_4 = [];
26 endStruct.Run_5 = [];
27 endStruct.Run_6 = [];
28 endStruct.Run_7 = [];
29 endStruct.Run_8 = [];
30 endStruct.Run_9 = [];
31 endStruct.Run_10 = [];
32 endStruct.Run_11 = [];
33 endStruct.Run_12 = [];
34 endStruct.Run_13 = [];
```

```matlab
35  endStruct.Run_14 = [];
36  endStruct.Run_15 = [];
37  endStruct.Run_16 = [];
38  endStruct.Run_17 = [];
39  endStruct.Run_18 = [];
40  endStruct.Run_19 = [];
41  endStruct.Run_20 = [];
42
43  for i = 1:length(runs)
44  % set run number
45  % run = i;
46  run = runs(i);
47      % assign data to each IMU
48  %     plot
49  % figure (i)
50  % hold on
51      for j = 1:12
52          data = getfield(SRunsIMUs, sprintf('Run_%d_IMU_%d'
              , run, j));
53          time = data(:,1);
54          accel = sqrt(data(:,3).^2 + data(:,4).^2 + data
              (:,5).^2);
55
56          endStruct = setfield(endStruct,sprintf('Run_%d',
              run),sprintf('IMU_%d',j),'time',time);
57          endStruct = setfield(endStruct,sprintf('Run_%d',
              run),sprintf('IMU_%d',j),'accel',accel);
58
59  %         1.  spline interp for 2 degrees of differentiable
        continuity
60  %         create a downsampled version in the
        ground_accel_data struct
61  %         L = floor((time(end)-time(1))*100)/100; %
        duration in time: floor of the 10ms (2nd decimal)
62  %         t = (0:1/Fs:L); % create evenly spaced time
        vector for interp
63  %         downsampled_data = interp1(time-time(1), accel,
        t,'spline');
64
65  %         2. use resample w/ built in anti-aliasing low
        pass filter
66  %         [downsampled_data, t] = resample(accel, time-
        time(1), Fs, 'spline');
67
68  %         3. use resample w/ built in anti-aliasing low
```

```matlab
         pass filter w/
69 %             spline
70 %             [downsampled_data, t] = resample(accel, time-time
      (1), Fs);
71
72 %             4. lowpass first then spline interp
73             L = floor((time(end)-time(1))*100)/100; % duration
                  in time: floor of the 10ms (2nd decimal)
74             t = (0:1/Fs:L); % create evenly spaced time vector
                  for interp
75             downsampled_data = interp1(time-time(1), lowpass(
                  accel,Fs, 100), t,'spline');
76
77
78 %             put into struct as time_d and accel_d
79             endStruct = setfield(endStruct,sprintf('Run_%d',
                  run),sprintf('IMU_%d',j),'time_d',t);
80             endStruct = setfield(endStruct,sprintf('Run_%d',
                  run),sprintf('IMU_%d',j),'accel_d',
                  downsampled_data);
81
82             clear data time accel L t downsampled_data % clear
                  for next it.
83         end
84 end
85
86 end
```

Fluidity calculation

```matlab
1 %% fludity calculations
2 % Data processing downsampled accel data into jerk and
      fluidity for
3 % analysis
4 % Author: Mich Lin (shuyulin)
5 % Date created: April 3 2023
6 % Date last modified: April 3 2023
7
8 function endStruct = fluiditycalc(trial, runs)
9
10 %% import data
11 if trial == 'flight'
12     load("flight_accel_data.mat", "flight_accel_data");
13     data = flight_accel_data;
14 elseif trial == 'ground'
```

```matlab
15        load("ground_accel_data.mat", "ground_accel_data");
16        data = ground_accel_data;
17 else
18        fprintf('need to enter flight or ground as string')
19 end
20
21 %% make new structs
22 endStruct.Run_1 = [];
23 endStruct.Run_2 = [];
24 endStruct.Run_3 = [];
25 endStruct.Run_4 = [];
26 endStruct.Run_5 = [];
27 endStruct.Run_6 = [];
28 endStruct.Run_7 = [];
29 endStruct.Run_8 = [];
30 endStruct.Run_9 = [];
31 endStruct.Run_10 = [];
32 endStruct.Run_11 = [];
33 endStruct.Run_12 = [];
34 endStruct.Run_13 = [];
35 endStruct.Run_14 = [];
36 endStruct.Run_15 = [];
37 endStruct.Run_16 = [];
38 endStruct.Run_17 = [];
39 endStruct.Run_18 = [];
40 endStruct.Run_19 = [];
41 endStruct.Run_20 = [];
42
43 %% calc jerk and fluidity and save to endStruct
44 for i = 1:length(runs)
45 % set run number
46 % run = i;
47 run = runs(i);
48      for j = 1:12
49 %          get the downsampled time
50          time_a = getfield(data,sprintf('Run_%d',run),
                sprintf('IMU_%d',j), 'time_d');
51          accel = getfield(data,sprintf('Run_%d',run),
                sprintf('IMU_%d',j), 'accel_d')/9.81;
52
53 %          preserve accel data
54          endStruct = setfield(endStruct,sprintf('Run_%d',
                run),sprintf('IMU_%d',j),'time_a',time_a);
55          endStruct = setfield(endStruct,sprintf('Run_%d',
                run),sprintf('IMU_%d',j),'accel',accel);
```

```matlab
56
57            time_j = time_a(2:end);
58            jerk = diff(accel)./diff(time_a);
59 %            put into struct as time_d and accel_d
60            endStruct = setfield(endStruct,sprintf('Run_%d',
                 run),sprintf('IMU_%d',j),'time_j',time_j);
61            endStruct = setfield(endStruct,sprintf('Run_%d',
                 run),sprintf('IMU_%d',j),'jerk',jerk);
62
63            time_f = time_j(1:end-1); % lhs num integration
64            dt = time_a(2)-time_a(1); % delta time for
                 integration
65            jerk_abs = abs(jerk); % absolute value so not
                 dividing by 0
66            fluidity = 1./((jerk_abs+1)); % this isn't correct
                  technically
67            fluidity_am = mean(fluidity); % arithmetic mean
68            fluidity_hm = length(fluidity)/sum(1./fluidity); %
                 harmonic mean
69
70            endStruct = setfield(endStruct,sprintf('Run_%d',
                 run),sprintf('IMU_%d',j),'time_f',time_f);
71            endStruct = setfield(endStruct,sprintf('Run_%d',
                 run),sprintf('IMU_%d',j),'fluidity',fluidity);
72            endStruct = setfield(endStruct,sprintf('Run_%d',
                 run),sprintf('IMU_%d',j),'fluidity_am',
                 fluidity_am);
73            endStruct = setfield(endStruct,sprintf('Run_%d',
                 run),sprintf('IMU_%d',j),'fluidity_hm',
                 fluidity_hm);
74
75
76            clear time_a accel time_j jerk time_f fluidity dt
                 fluidity_mag % clear for next it.
77       end
78 end
79 end
```